

Thermal weakening friction during seismic slip: an efficient numerical scheme for heat diffusion

S. Nielsen¹, E. Spagnuolo², M. Violay³ and G. Di Toro⁴

¹Department of Earth Sciences, Durham University, *DH1 3LE* Durham, United Kingdom

²Istituto nazionale di Geofisica e Vulcanologia, Via di Vigna Murata, 605, *00143* Roma, Italy

³EPFL ENAC IIC LEMR, GC D1 401 (Bâtiment GC), Station 18, *CH-1015* Lausanne, Switzerland

⁴Dipartimento di Geoscienze, via G. Gradenigo, 6, *35131* Padova, Italy

Key Points:

- Thermal diffusion can be solved efficiently through a parsimonious numerical scheme
- Thermal weakening models of seismic friction work best if the evolution of background temperature during slip is included
- Both heat source (friction) and heat sinks (decomposition reactions) should be included in the temperature computation to reproduce accurately weakening and restrengthening

Abstract

Recent experiments systematically explore rock friction under crustal earthquake conditions (slip velocity $V \geq 1$ m/s and normal stress $5 < \sigma_n < 50$ MPa), revealing that faults undergo abrupt dynamic weakening. Processes related to heating and weakening of fault surface asperities, plastic yielding or frictional melting have been invoked to explain pronounced velocity weakening. Both asperity temperature T_a and background temperature T of the slip zone evolve significantly during high velocity slip due to heat sources (frictional work), heat sinks (e.g. latent heat of decomposition processes) and diffusion. Tracking the evolution of T accurately in a numerical scheme can be quite costly. Therefore we propose an accurate and parsimonious scheme for the solution of temperature, resulting in a compact formula with a small number of memory variables. This can allow the efficient integration of T in dynamic models of rupture on an extended fault. Using T as a state variable, we seek appropriate frictional forms for use in seismic dynamic rupture models. We test the compatibility of thermal weakening models with carefully calibrated High Velocity Rotary Friction experiments. (1) Models of friction based only on T in an extremely simplified, Arrhenius-like thermal dependence, reproduce the gross features of the frictional weakening. (2) A flash heating law which accounts for evolution of both V and T , including heat sinks in the thermal balance. The presence of dissipative heat sinks significantly affects the diffusion solution for T and reflect on the friction, allowing a better fit of the strength recovery observed in the experiments.

Plain Language Summary

During earthquakes, fast slip on the fault generates large amounts of localized heat. The consequent temperature rise has been proposed as one main cause of abrupt frictional weakening, concomitant with decomposition reactions, which act as heat sinks, partially buffering the temperature rise. Here we test two models of thermal weakening by computing the temperature evolution and the temperature-dependent friction including the heat sinks and the heat diffusion. Tracking the evolution of temperature with a variable heat source can be quite costly in a numerical scheme, so we design a parsimonious scheme using wavenumber summation which is accurate and extremely efficient.

1 Introduction

Well-studied Dieterich-Ruina rate-and-state laws (Dieterich, 1979; Ruina, 1983; Marone, 1998) describe accurately the friction under slow, aseismic creep. However, it has been long

46 recognized in models of earthquake rupture that it is necessary to account for the presence of
 47 more radical dynamic weakening at high slip velocity. In a few cases, it has been possible to
 48 constrain some aspects of co-seismic sliding friction: absolute stress level was obtained us-
 49 ing rake rotation of slip during the Kobe, 1995 earthquake (striation, absolute stress, inversion,
 50 source, 1998), or the rotation of focal mechanisms in small earthquakes before and after the
 51 main rupture of Tohoku, 2011 earthquake (Hasegawa et al., 2011); both cases indicated that
 52 the sliding friction must have been extremely low. In addition, a very low temperature increase
 53 was measured months after the Tohoku earthquake in a borehole across the fault, again com-
 54 patible with low co-seismic sliding friction (Fulton et al., 2013). Finally, a weakening distance
 55 of $\approx 1.5\text{--}1.7$ m was estimated using strong-motion records containing mach waves from the
 56 Denali, 2002 and the Izmit, 1999 earthquakes (Cruz-Atienza & Olsen, 2010). In spite of such
 57 rare highlights, dynamic weakening remains difficult to quantify based on seismological earth-
 58 quake data. Hence a number of laws with enhanced velocity-weakening have been implemented
 59 in models of seismic fault rupture (dynamic, 1998; Nielsen & Madariaga, 2003; Noda et al.,
 60 2009), relying mostly on theoretical arguments (Archard, 1959; J. R. Rice, 2006; Rempel &
 61 Rice, 2006; Rempel & Weaver, 2008; Beeler et al., 2008; Nielsen et al., 2008; Noda et al., 2009,
 62 and references therein).

63 On the other hand, an increasing number of well-constrained observations are being ob-
 64 tained in laboratory experiments performed under close to co-seismic conditions. Yuan and
 65 Prakash (2008, 2012) used an impact bar to load impulsively a frictional slip surface under
 66 extreme conditions of slip rate (tens of meters per second) and normal stress (hundreds of Mega
 67 Pascals) while measuring the shear resistance to slip; they found an abrupt weakening occur-
 68 ring over extremely short slip distances ($< 1\mu\text{m}$) and times ($< 1\mu\text{s}$). Intermediate, more seismic-
 69 like conditions were studied (0.5-6.5 m/s, 1-50 MPa) using rotary shear machines (Tsutsumi
 70 & Shimamoto, 1997; Di Toro et al., 2004; Hirose & Shimamoto, 2005; Di Toro et al., 2006;
 71 Han et al., 2007; Mizoguchi et al., 2007; Fondriest et al., 2013; Sone & Shimamoto, 2009; Vi-
 72 olay, Nielsen, Gibert, et al., 2013; Violay et al., 2015) also showing in pronounced weaken-
 73 ing; however, in the latter experiments the measured weakening distances were much longer
 74 (of the order of tens of centimeters to several meters).

75 In the case of frictional melting the role of temperature and frictional power in the weak-
 76 ening were directly modeled, and it was shown that the weakening was accelerated under larger
 77 normal stress and slip velocity (Nielsen, Mosca, et al., 2010). Theoretical arguments (Nielsen
 78 et al., 2008) predicted that the final, steady-state friction level depended on normal stress to

a power $1/4$, which was later confirmed by accurate experiments (Violay et al., 2014). The center of the molten layer can reach peak temperatures well above those of melting temperatures of the rock-constituent minerals (overheating), creating an ultra-thin, ultra-low viscosity slip layer whose lubricant effect is all the more efficient than slip rate and normal stress are elevated. However previous modelling of frictional melt during the transient weakening (Nielsen, Mosca, et al., 2010) relies on a complex, explicit numerical model; in addition, the model considers cases where melting is observed (in silica-built rocks) but not the cases where no melting occurs –e.g., carbonatic rocks, (Han et al., 2007; Violay, Nielsen, Spagnuolo, et al., 2013)– although, there too, considerable weakening takes place. Thermal pressurization of fluids confined to a narrow fault zone has also been invoked as a cause for profound weakening in natural faults (Rempel & Rice, 2006; J. R. Rice, 2006). Such mechanism may take place in fluid-saturated, relatively low permeability fault zones, and modelling shows that it can be compatible with the estimates of fracture energy from natural earthquakes (J. R. Rice, 2006; Viesca & Garagash, 2015). In a few cases, high-velocity experiments were conducted with fluids under drained and undrained conditions, on bare rock samples with no gouge, showing the onset of thermal pressurization only in the later phases of slip where friction was already considerably low (Violay, Nielsen, Gibert, et al., 2013; Violay et al., 2011; Violay, Nielsen, Spagnuolo, et al., 2013; Violay et al., 2015). However it is observed in most high-velocity friction experiments that extremely fast, efficient weakening takes place on natural rocks even in the absence of fluids.

Drawing on early studies of flash heating of asperities in metal friction (Archard, 1959), Rice (J. Rice, 1999; J. R. Rice, 2006) introduced a model where rock friction at high slip rates where temperature rise is implicit and the asperities weakening is essentially related to slip velocity; such flash-weakening model was subsequently discussed by Beeler et al. (2008) and Rempel and Weaver (2008).

It has been claimed that slip acceleration (Chang et al., 2012) plays a fundamental role in dynamic friction reduction; however, combined high slip velocity and high normal stress, producing high frictional power, appear to be the key requirements to induce pronounced weakening (Di Toro et al., 2011) independently of the imposed acceleration. In fact one direct consequence of elevated frictional power is to induce an elevated and localized temperature growth on the slip surface and its immediate vicinity; accordingly high temperature has been indicated as a likely cause of dynamic frictional weakening. On the other hand, the direct effect of temperature on the weakening may be questioned. Experiments conducted on preheated samples

of dolerite (Noda et al., 2011) with the use of a furnace, and on Westerly granite, India gabbro and quartzite (Noda et al., 2011; Passelègue et al., 2014), reveal a correlation between weakening and temperature, independently of slip velocity, although the weakening is relatively modest. Frictional weakening of pre-heated olivine samples at slow slip rates is even more modest (King & Marone, 2012). We shall discuss these results here in terms of localized versus background temperature changes.

Here we discuss aspects of frictional contact and the effects of heating under high-velocity sliding. We define a model which starting point is based on the flash-weakening formalism discussed above (Archard, 1959; J. Rice, 1999; J. R. Rice, 2006; Beeler et al., 2008; Rempel & Weaver, 2008), and extend it to include the effect of frictional heating on the background temperature, thermal diffusion, and the presence of heat sinks due to decomposition or melting. We propose an extension to account for the onset of frictional melting and shortening. We indicate a parsimonious numerical scheme for the temperature update. Assumptions and approximations are used in order to obtain a sufficiently elementary and uncomplicated model for practical use as a friction law in earthquake slip models, while retaining the essential behavior observed during rock test experiments under coseismic conditions.

Temperature evolution is important in the weakening behaviour, but its accurate numerical evaluation can be costly and inefficient over an extended number of time steps. Such cost may become prohibitive when the temperature needs to be evaluated at many different points in an extended fault model. Here we propose a fast and efficient temperature computation scheme based on a wavenumber decomposition, where a small number of memory variables are updated at each iteration. Accuracy within a few percent can be achieved with a small number of memory variables (16 or less), and can be augmented to an arbitrary level by increasing the number of memory variables. The scheme is easily implemented in any programming language and can be integrated in existing numerical codes.

The models are calibrated and tested against a number of selected rotary shear, high-velocity experiments performed on the SHIVA machine hosted at Istituto Nazionale di Geofisica e Vulcanologia, Roma. We used hollow cylindrical samples of 30/50 mm inner/outer diameter, respectively, machined from gabbro (as a representative of silicate-built rocks) and Carrara marble (as a representative of carbonate-built rocks). The experimental conditions cover the range from 10–30 MPa in normal stress and from 1–6.5 m/s in slip velocity.

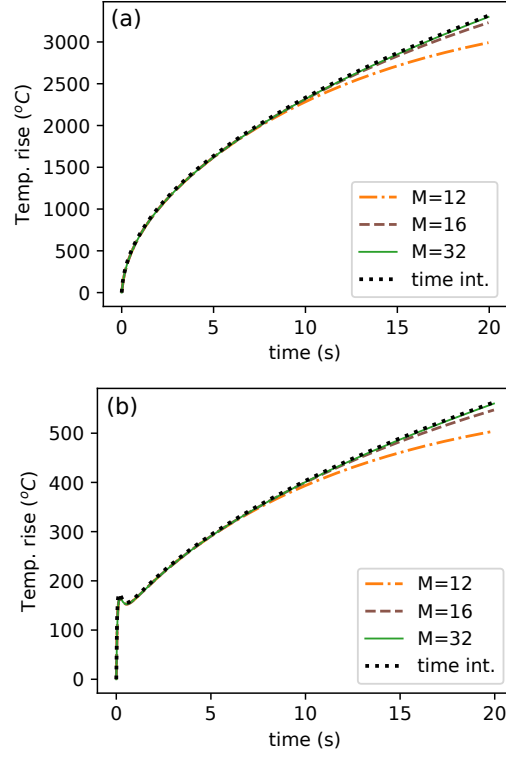


Figure 1. Test of the parsimonious scheme (wavenumber summation eq. 19). Temperature evolution is shown for (a) constant heat flux ($3 \times 10^6 \text{ J m}^{-2} \text{ s}^{-1}$) and (b) exponentially decaying heat flux ($5 \times 10^5 + 3 \times 10^6 \exp(-10t)$). Solutions are shown for $M = 12, 16, 32$ (dot-dashed, dashed and solid curve, respectively). For comparison, the solution obtained from the direct discretization (8) of the analytical solution (time integral) is shown (dotted curve). The time stepping is $dt = 0.04$. See text for further details.

2 Heat sources and sinks

The frictional work released per unit time per unit area on the sliding interface is

$$q_f = \tau(t) V(t) \quad (1)$$

where V is the slip rate and τ a macroscopic average of the shear stress. Frictional work is responsible for temperature rise, but it is in part dissipated by thermal diffusion and in part by other endothermal processes (latent heat for melting, decomposition, heat removal by fluid mass escape from the interface, surface energy involved in comminution, etc.). The latter processes are known to act as a buffer which inhibits the continuous rise of temperature; we argue that they have a significant effect on the background temperature and friction.

Assuming that the frictional heat rate from (1) takes place on the fault surface (or within a principal slip zone of negligible thickness) at $z = 0$ and propagates away from the fault surface, we may write the one-dimensional thermal diffusion equation

$$\partial_t T = \kappa \partial_z^2 T + \frac{\delta(z) q}{\rho c} \quad (2)$$

where $\delta(z)$ is the Dirac delta function, ρ is mass density, and c heat capacity. The net heat source q can be described as the difference between frictional heating q_f and the sinks q_s :

$$q(t) = 1/2 (\tau(t) V(t) - q_s(T(t))) \quad (3)$$

where the $1/2$ factor indicates that the available heat will propagate on both sides of the fault.

Finally, the shear stress τ arises from the sliding friction, which is arguably a function of sliding rate V , temperature T , and any number of state variables:

$$\tau(t) = f(V, T, \dots) \quad (4)$$

We delay to section (6) the discussion of particular forms of (4) including thermal dependence, and their compatibility with observed experiments of high velocity friction, and discuss here the nature of possible heat sinks.

The temperature-limiting effect of thermal decomposition has been modeled explicitly in the case of carbonatic rocks (Sulem & Famin, 2009), gypsum (Brantut et al., 2010) and dolomite with application to the emplacement of a giant landslide (Mitchell et al., 2015). Generally the kinetics of a reaction is accelerated exponentially with temperature (Arrhenius kinetics), as a consequence the rate of latent heat loss should increase likewise. In the case of experiments performed in the open air there is a Newtonian radiative loss which is generally considered

as proportional to temperature. Finally, in the presence of a cooling fluid circulation there should also be a heat loss proportional to temperature due to convection (Violay, Nielsen, Gibert, et al., 2013; Acosta et al., 2018).

Heat loss due to constant flow rate of cooling fluid may be approximated as $q_s = \psi (T - T_i)$ per unit time, assuming that fluid enters the interface at T_i (ambient rock temperature) and exits at temperature T (background interface temperature); ψ is the heat capacity of the fluid times its flow rate (per unit area). Heat loss due to decomposition processes will be represented by an exponential Arrhenius law of the form (Sulem & Famin, 2009):

$$q_s = \alpha (1 - n) h \rho L A \exp\left(-\frac{E_a}{RT}\right) \quad (5)$$

Here h is the thickness of the zone affected by the decomposition, $(1 - n)$ is the remaining proportion of (unreacted) material (in first approximation $1 - n \approx 1$) and $R = 8.31 \text{ J K}^{-1} \text{ mol}^{-1}$. Note that in eq. (5) T is absolute temperature, but in the following sections T is the excess above initial temperature. In the example of decarbonation of pure calcite, indicative literature values (Sulem & Famin, 2009) are $E_a = 319 \cdot 10^3 \text{ J/mol}$, $A = 2.95 \cdot 10^{15} \text{ s}^{-1}$, $L = 3190 \cdot 10^3 \text{ J/kg}$, for activation energy, pre-exponential factor and latent heat, respectively, $\rho = 3000 \text{ kg m}^{-3}$ and $R = 8.31$. Defining $C_s = (1 - n) h \rho L A$ and $T_s = E_a/R$, we may re/write the heat loss as

$$q_s = C_s \exp(T_s/(T + T_i)) \quad (6)$$

We note that the term $q_s(T(t))$ in equation (3) implicitly describes heat sinks that are distributed over a finite thickness h . Distributed heat sinks can be explicitly included using the values of temperature and temperature gradient away from the sliding surface which are derived in equations (21-20). However here for simplicity we will assume that the temperature over h can be equated to that of the sliding surface $T = T(z = 0)$, and that h is constant; a similar approximation was also used in Mitchell et al. (2015).

In the case of frictional melt, the latent heat and melt extrusion have been taken into account explicitly to model temperature evolution and to describe frictional behavior in both steady-state (Nielsen et al., 2008) and transient conditions (Nielsen, Mosca, et al., 2010). In the case of pervasive melting, it is necessary to solve the Stefan problem with an added term of mass transport in (2), a case also discussed further in section 6.3 and in Appendix.

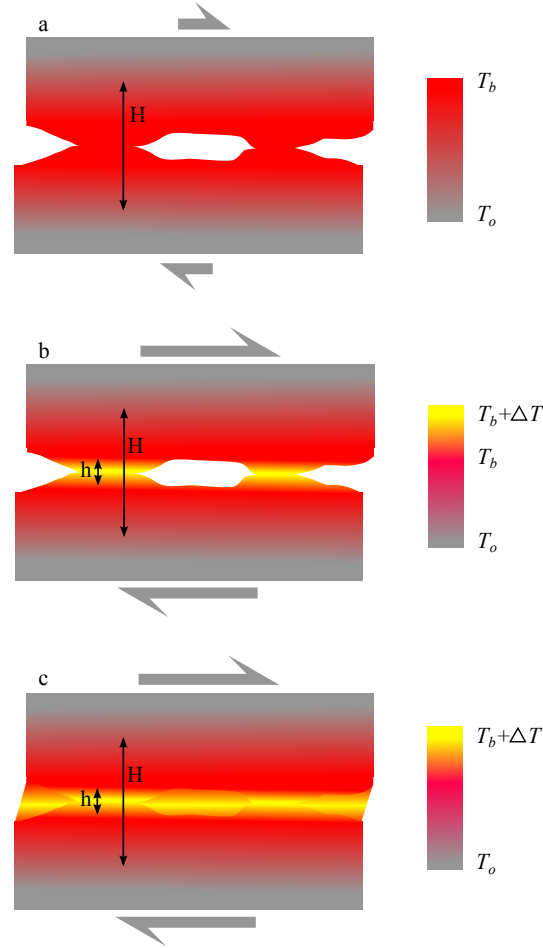


Figure 2. Schematic temperature distribution in the slip zone. (a) Slow velocity: the heat diffuses beyond the asperity size during the lifetime of a contact, temperature rise is homogeneous within H . The temperature T_b is evenly distributed, so that weakening is compensated by the growth of contact area. High velocity: (b) the asperity undergoes a local, transient temperature rise ΔT which diffuses within a limited thickness h during the short contact lifetime; on timescales of multiple contacts the heat diffuses throughout thickness H and background interface temperature rises to T_b . Temperature is unevenly distributed; the weakening due to highly localized temperature $T_b + \Delta T$ surpasses the friction increase due to the growth of contact area under an average interface temperature T_b . (c) A pervasive layer of overheated, lubricant material has formed with peak temperature $T_b + \Delta T$ within the layer and weakening is efficient.

3 Temperature computation

Frictional sliding can generate temperature peaks at local contact asperities and also a general rise of background temperature of the sliding surface (see discussion of section 4). We provide a number of indications that background temperature plays an important role in the weakening (section 5). Therefore its computation is of paramount importance in problems of thermal weakening.

The problem of heat diffusion is well-known and a number of analytical and numerical solutions have been proposed. However to our knowledge the relative low speed and efficiency of current numerical solutions can be quite limiting in a problem where temperature needs to be computed repeatedly at many different points (as in the case of dynamic rupture models). We propose in (3.2) an extremely efficient a wavenumber formulation, which solution consists in the update and summation of a small number of memory variables.

3.1 Direct (inefficient) temperature computation

One well-known (Carslaw & Jaeger, 1959) solution of eq. (2) is

$$T(t) = \gamma \int_0^t \frac{q(t')}{\sqrt{t-t'}} dt', \quad (7)$$

where $\gamma = (2\rho c\sqrt{\kappa\pi})^{-1}$ (with mass density, heat capacity and thermal diffusivity ρ , c and κ , respectively). t is current time and t' is the integration variable). Direct discretization of (7) with time step δt yields at the n_{th} iteration (time $t = n\delta t$):

$$T(n) = \gamma \sum_{i=1}^n \frac{q(i)}{\sqrt{\delta t \times (n - 1/2 - i)}} \delta t. \quad (8)$$

Although solution (8) may be used to compute temperature, we propose a practical approximation in order to reduce substantially the computational cost. Indeed (8) requires a summation over all past time iterations at each time step, so that the number of computations grows with time. In case that small time steps are required, and an extended fault is modeled with inhomogeneous distribution of T and τ , the computation may become prohibitively long. Typical simulations would require the memory storage of a number of time iterations in excess of several thousands. Noticing that equation (7) is a convolution on may suggest the use of FFT (Fast Fourier Transform) in time. However, the operation would still imply several thousand time iterations n and normally requires that n is a power of 2. Finally, The operation and the storage would be take place at each of the subsegment of the modeled fault, which easily exceed the thousands. In conclusion, it is necessary to design an adequate approximation

of the thermal diffusion. In the section below we propose a straightforward time iterative scheme, where the temperature is computed to a satisfactory approximation by the use of a small number of memory variables which arise in a discrete wavenumber solution.

3.2 Wavenumber (efficient) temperature computation

The one dimensional heat diffusion equation (2) with a heat source flux $q = q(t)$ at $x = 0$ per unit time per unit area, which we re-write here for convenience, states:

$$\partial_t T = \kappa \partial_z^2 T + \frac{\delta(z) q}{\rho c} \quad (9)$$

where $\delta(\cdot)$ is the Dirac delta function and z is the distance from the slip surface. Taking the wavenumber transform $z \rightarrow s$, we note that the temperature is an even function of z and – expecting no singularities – we may use the Cosine Fourier transform (using only the positive real wavenumbers) to obtain

$$\partial_t \theta(s, t) = \frac{q(t)}{\rho c} - \kappa s^2 \theta(s, t) \quad (10)$$

where $\theta(s, t)$ is the wavenumber Fourier transform of $T(z, t)$.

For consistency, we show in Appendix II how the analytical expression of temperature (7) can be retrieved by solution of (10) and the subsequent inverse cosine transform.

However here we directly update θ using a discrete wavenumber summation. For the discrete version of time-iterative scheme it is better to select a backward Euler stepping scheme to insure stability (backward meaning that the updated value $\theta(s, t)$ is both on the right- and left-hand side of the equation):

$$\frac{(\theta(s, t) - \theta(s, t - \delta t))}{\delta t} = \frac{q(t)}{\rho c} - \kappa s^2 \theta(s, t) . \quad (11)$$

to the first order of the series expansion. By regrouping terms we obtain the updated value as

$$\theta(s, t) = \left(\frac{q(t) \delta t}{\rho c} + \theta(s, t - \delta t) \right) \frac{1}{1 + \delta t \kappa s^2} . \quad (12)$$

The update of $\theta(t)$ is obtained from the former value $\theta(t - \delta t)$ plus the scaled heat rate, divided by a constant function of wavenumber s . Importantly, the summation does not require all past times, but only the value of θ from the former time step. The inverse transform (i.e., summation over s) yields temperature such that:

$$T(x, t) = \frac{2}{\pi} \int_0^\infty \cos(s z) \theta(s, t) ds, \quad (13)$$

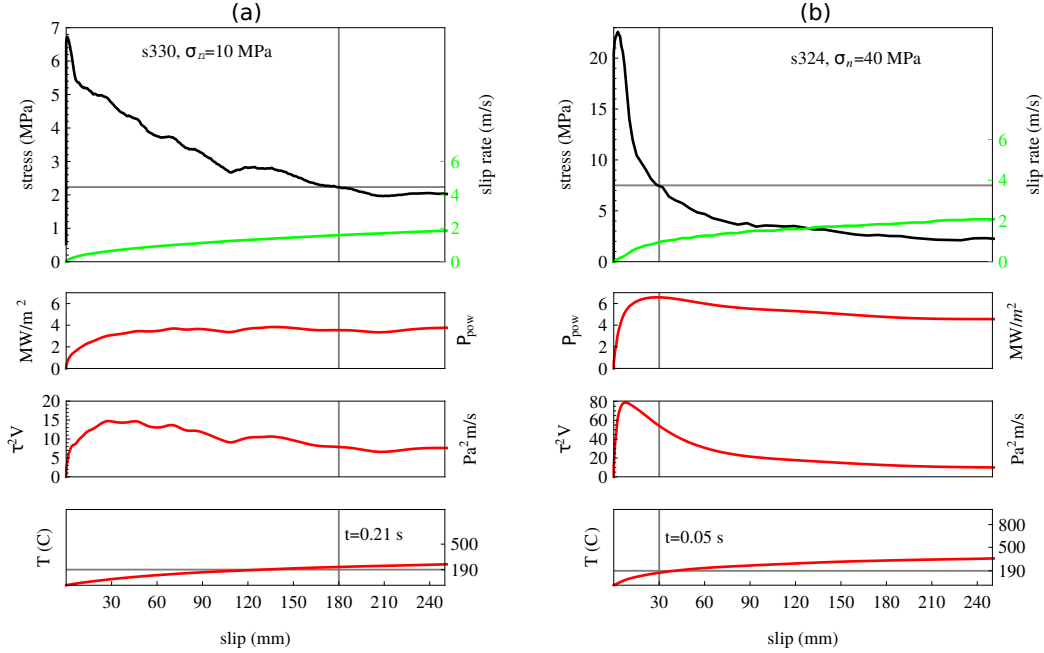


Figure 3. Comparison of two sliding friction experiments on precut Carrara marble performed under identical conditions except for normal stress (10 and 40 MPa, respectively). The weakening curve, the slip velocity, power and the product $\tau^2 V$ are shown in both cases. (a) Experiment s330 performed at normal stress 10MPa. The shear stress drops to 1/3 of the peak value (indicated by horizontal line) during the initial 0.21 s and 180 mm of slip (vertical line), with average values $\overline{\tau^2 V} \approx 12 \text{ Pa}^2\text{m/s}$. (b) Experiment s324 performed at normal stress 40MPa. Shear stress drops to 1/3 of the peak value during the initial 0.05 s and 30 mm of slip, with average values $\overline{\tau^2 V} \approx 70 \text{ Pa}^2\text{m/s}$. A factor of six reduction in the weakening distance corresponds roughly to a factor of six increase in $\overline{\tau^2 V}$, which is expected if weakening is related to temperature increase. Similarly, the factor of two reduction in average power $\overline{\tau^2 V}$ results in a factor of four increase in time (0.21 and 0.05 s, respectively) to reach equivalent weakening. A similar background temperature increase ($T \approx 190^\circ\text{C}$) above initial ambient temperature ($T = 20^\circ\text{C}$) is estimated in both experiments at 1/3 weakening; however, a background temperature $T \approx 210^\circ\text{C}$ is much lower than that expected to trigger weakening by decomposition reactions in calcite (about 600°C). See text for further details.

and at $z = 0$:

$$T(0, t) = \frac{2}{\pi} \int_0^\infty \theta(s, t) ds. \quad (14)$$

For the numerical solution we also discretise the wavenumbers by steps δs . We shall use the notation $\theta_m(t) = \theta(m \delta s, t)$ with $(1 < m < M)$ where M is the total number of discrete wavenumbers. Thus (14) yields:

$$T(t) = \frac{2}{\pi} \sum_{m=1}^M \theta_m(t) \delta s \quad (15)$$

and each θ_m variable will be computed according to (12) such that

$$\theta_m(t) = \left(\frac{q(t) \delta t}{\rho c} + \theta_m(t - \delta t) \right) \frac{1}{1 + \delta t \kappa s_m^2},$$

where

$$s_m = (m - 1/2) \delta s. \quad (16)$$

As discussed below a rather small summation number M is sufficient. The time integration has disappeared, replaced by a more convenient summation over a small number of memory variables from the previous time step. The constitutive relation may be now written as (1) a friction law based on M memory variables and (2) an evolution law for the memory variables:

$$\tau(t) = f(\theta_1 + \theta_2 + \dots \theta_M, V, \dots) \quad (17)$$

$$\partial_t \theta_m = \frac{q(t)}{\rho c} - \kappa s_m^2 \theta_m \quad (\text{where } s_m = (m - 1/2) \delta s) \quad (18)$$

The memory variables here have temperature dimension (as opposed to time dimension in the case of Dieterich-Ruina rate and state evolution friction laws). The interpretation of the solution in memory variables corresponding to different wavenumbers is straightforward: largest wavenumbers represent the fast temperature evolution due to thin penetration depth of heat, while the small wavenumbers represent the slower temperature evolution due to larger penetration depth.

Using (15) rather than (8) will require a fixed, limited number M of memory variables in a short summation as opposed to an ever increasing number temperatures stored from each previous timestep (see example below, with $M = 16$ and $M = 32$).

223

In a nutshell: the temperature update scheme

Finally, we may sum-up the iterative scheme as follows. Upon discretization in time steps of size δt and M wavenumber steps of size δs , the memory variables θ_m are updated at each time iteration n , and summed in order to obtain the current temperature T according to:

$$\begin{aligned}\theta_m &= \left(\frac{q(n)}{\rho c} \delta t + \theta_m^- \right) \frac{1}{1 + \delta t \kappa s_m^2} \\ T(n) &= \frac{2}{\pi} \sum_{m=1}^M \theta_m \delta s\end{aligned}\tag{19}$$

where θ_m^- is the m_{th} memory variable from the previous time step and s_m is defined in eq. (16).

The above temperature T can then be used to update the temperature-dependent stress according to eq. (28). If the gradient of the temperature is required it can simply be obtained by

$$\partial_z T(t) = \frac{2}{\pi} \sum_{m=1}^M s_m \theta_m \delta s\tag{20}$$

and temperature at a distance z from the source (fault plane) is obtained simply by:

$$T(z, t) = \frac{2}{\pi} \sum_{m=1}^M \cos(z s_m) \theta_m \delta s\tag{21}$$

224

225

226

227

228

229

230

231

232

233

234

An adequate choice of s sampling is critical to achieve a good solution with a minimum number M of discrete wavenumbers s (and memory variables θ). Let's assume that the duration of interest is t_c and that we wish to obtain an approximate solution based on M wavenumbers. An indicative penetration depth for diffusion problems is $z_{max} \approx D\sqrt{\kappa t_c}$, where D is a dimensionless constant. We can use this formula to estimate a maximum wavelength in the problem, and we found that a good rule of thumb is $D = (2/5)M$. This rule may appear counter-intuitive, because the consequence of increasing M is to improve the sampling at small wavenumbers (long wavelengths) rather than at large wavenumbers. However the larger error in this method is found at later times and larger scales. Therefore extending the sampling toward low wavenumbers provides the maximum improvement. The minimum wavenumber is fixed by $s_{min} = 2\pi/z_{max} = 5\pi/(M\sqrt{\kappa t_c})$.

235

236

237

The minimum wavelength in the problem will be determined by the number of wavenumbers M such that $z_{min} = z_{max}/(2M)$ (i.e., in the center of the first wavelength interval). As a consequence, the maximum wavenumber is fixed by $s_{max} = 2\pi/z_{min} = 10\pi/\sqrt{\kappa t_c}$.

238

239

The wavenumber sampling step is $\delta s = s_{max}/M = 10\pi/(M\sqrt{\kappa t_c})$, and the sampling will take the form $s = (m - 1/2)\delta s$, $1 < m < M$.

240

241

For a practical example, let's use $t_c = 20$ s, $\kappa = 1.1 \cdot 10^{-6} \text{m}^2 \text{s}^{-1}$, $\rho = 3000$, $c = 715$ $\delta t = 0.04$, $N = 500$. The discrete wavenumber solution is derived using $\delta s = 10\pi/(M\sqrt{\kappa t_c}) = 209.3 \text{ rad m}^{-1}$,

and the sample wavenumbers are $s_m = (m - 1/2) \delta s$, where $(1 < m < M)$, which results in $s_m = (104.7, 313.96, 523.27, \dots)$. In Fig. (1) we show the results for three different samplings, $M = 12$, $M = 16$ and $M = 32$. For reference we also show the result of time summation (eq. 8), which is a direct discretization of the analytical solution (7). Solutions are derived for either a constant heat flux ($q = 3 \text{ MJ m}^{-2}\text{s}^{-1}$) or an exponential decay ($q = 0.5 + 3 \exp(-t/0.1) \text{ MJ m}^{-2}\text{s}^{-1}$).

For most practical purposes, $M = 16$ yields a satisfying approximation (with a precision of a few percent after $t = 20 \text{ s}$). $M = 32$ yields a result which differs less than 1/10000 at $t = 20 \text{ s}$ when compared to the classic solution obtained by direct discretization (2). Timing the computation example above with $M = 16$ (on a desktop computer with python) yields 8.44 ms for the wavenumber solution versus 132 ms for the classic time summation, and storage of 16 floating point values versus 500, i.e. an estimated gain of 97% in CPU time and 94% in memory storage.

An example of code for temperature computation is provided in Supplementary Materials.

4 Nature of the frictional interface

4.1 Real and nominal contact area

Shear and normal stress across the sliding interface are supported by local asperities whose real contact area A_r represents only a small fraction α of the nominal area A_n . During slip, asperity contacts coalesce, deform and disappear forming a distribution at various stages of evolution and under continuous renewal. Because rock constitutive minerals yield under a few percent of strain, within each asperity the shear stress reaches the yield point early during its contact lifetime.

After yielding each asperity deforms under either brittle failure or creep, possibly at very high strain rate; however it cannot support a stress value much in excess of the yield value, lest yielding would propagate from the asperity into the supporting substrate thus keeping the stress value bounded. Hence the majority of asperities is close to the yield shear stress τ_y which can be considered as an average asperity value. The bulk frictional force resisting slip can be written as $F = A_r \tau_y$ which, normalized by A_n , yields the bulk frictional stress:

$$\tau = \alpha \tau_y. \quad (22)$$

α results from the ratio of applied normal stress σ_n to indentation hardness σ_c (or penetration hardness according to (Persson, 2000), Chapter 5.1) such that

$$\alpha = \sigma_n / \sigma_c \quad (23)$$

but in any case $\alpha \leq 1$ so that we may write $\alpha = \text{Min}[1, \sigma_n / \sigma_c]$.

We remark that both indentation hardness (Atkins & Tabor, 1965; Hirth & Kohlstedt, 2004; King & Marone, 2012) and yield shear stress (Weidner et al., 1994; Raterron et al., 2004) are observed to have a strong negative temperature dependence. Accordingly, an increasing temperature induces a decrease in τ_y but an increase in α —see also discussion in (Hirth & Beeler, 2015, and references therein). An increase in the area of asperity contact has been documented, for example, in olivine under slow slip velocity (King & Marone, 2012). Since the thermal weakening and contact area increase have antagonistic effects, the temperature dependence of bulk friction τ is not trivial to predict. In fact experiments performed under slow slip velocity do not show a systematic or pronounced frictional drop with temperature (Noda et al., 2009; King & Marone, 2012).

However under high slip velocity a pronounced weakening is observed in correspondence of the temperature rise at the interface. First, we shall propose how to reconcile these two conflicting observations based on the role of slip velocity and temperature localization. Then we shall proceed to the computation of the bulk frictional resistance of the interface based on local, temperature-dependent rheology.

In case that a pervasive lubricant layer develops and fills continuously the space between the asperity contacts (for example a pervasive melt layer, (Nielsen, Di Toro, & Griffith, 2010)) and supports the bulk of shear and normal stress, the temperature effect on α is buffered as we may consider $\alpha \approx 1$. At this point $\tau_y = \tau$ is the viscous shear stress supported by the lubricant layer within a principal slip zone (PSZ), and resistance to sliding is due to the viscous shear of a thin melt layer. Though the heating is not localized at the asperity contacts, it is still localized and concentrated within a thin shear layer provided that slip is brief enough (earthquake-like duration, typically seconds) that heat diffusion away from the PSZ is reduced (close to adiabatic conditions). In a different context (no melting) Cornelio et al. (2019, 2020) have shown how viscous fluids permeating natural rock samples affect frictional weakening at high slip velocity by activating elasto-hydrodynamic lubrication.

4.2 Shear thickness and shear rate

Observations on paleoseismic faults which were active at epicentral depths (≈ 10 km, (Di Toro et al., 2005)) show that slip often localizes within a PSZ of limited thickness (of the order of $100 \mu\text{m}$ or less). Active or fossil faults at moderate depths also often exhibit localized principal slip zones within a wider fault core (Sibson, 2003; Otsuki et al., 2003; J. R. Rice, 2006; De Paola et al., 2008; Collettini et al., 2011, and references therein).

Finally, laboratory experiments conducted under high stress and velocity also report the development of extremely thin PSZs either between two consolidated rock samples or within simulated or natural fault gouge. In the latter case localization is achieved only after a critical slip of several centimeters (Smith et al., 2015; Pozzi et al., 2018, 2019). The strain rate can be equated either to the ratio of slip velocity to the thickness of the PSZ, in the presence of a pervasive lubricant layer, or in the absence thereof, to the ratio of the slip velocity to asperity height (typically $\approx 10 - 100 \mu\text{m}$).

Since average seismic fault slip velocity estimated during earthquakes is typically $V \approx 1 \text{ m/s}$, the resulting shear strain rate within the PSZ or within the asperity contacts is extremely high ($\dot{\epsilon} = V/10^{-4} = 10^4 \text{ s}^{-1}$) and is associated to a number of thermally triggered decomposition, alteration or amorphization processes (dehydration, melting, decarbonation, stress corrosion, comminution, ...) which may directly or indirectly affect friction through the action of pressurization and/or the formation of a lubricant layer (Hirose & Shimamoto, 2005).

4.3 Arrhenius thermal dependance and flow stress

While little is known about rock rheology at large strain rates, stress relaxation occurs through any of i different crystal plastic mechanisms (dislocation diffusion, grain boundary migration, ...) which generally obey standard Arrhenius thermal dependence with activation energy Q_i and a power dependence on stress such that :

$$\dot{\epsilon} = A_1 \tau^{n_1} \exp \frac{-Q_1}{RT} + \dots + A_i \tau^{n_i} \exp \frac{-Q_i}{RT} \quad (24)$$

where the constants A_i may include a grain size dependence for particular deformation mechanisms (e.g. diffusion plasticity). Within a given range of stress and temperature, we may assume that a single mechanism will dominate and invert it to obtain

$$\tau_y = C \dot{\epsilon}^{\frac{1}{n}} \exp \frac{Q}{nRT} \quad (25)$$

where σ , $\dot{\epsilon}$ are the stress and the shear strain rates, respectively and T is the temperature. The exponent may be as low as $n = 1$ for some purely diffusive processes (Nabarro-Herring, (Poirier, 1985)) but in most cases $n > 1$; for example, $n = 2$ for grain boundary sliding (Karato, 2008) and typical values $1.5 < n < 3$ are observed at $\dot{\epsilon} = 10^3 - 10^4$ in experiments on ceramics in brittle conditions (Lankford, 1996). The term C ($\text{Pa s}^{1/n}$), though considered constant here for simplicity, may be strongly dependent on grain size (e.g. in the case of grain boundary sliding) among other parameters (Violay et al., 2012). A consequence of $n > 1$ is that the $\dot{\epsilon}^{1/n}$ term does not vary greatly under extremely elevated values of strain rate (e.g., the term $\dot{\epsilon}^{1/3}$ varies of about 25% upon a twofold increase of slip velocity from 1 m/s to 2 m/s, assuming a shear zone of $100\mu\text{m}$). On the other hand, expected temperature changes of a few hundred degrees may induce a huge variation in the exponential dependence. As a consequence, under high slip velocity we can expect that the variation of τ_y is primarily due to temperature changes and, for simplicity, we may neglect the variability of $\dot{\epsilon}^{1/n}$ to write

$$\tau \approx \alpha \tau_a \exp^{\frac{T_c}{T+T_i}} = \tau_0 \exp^{\frac{T_c}{T+T_i}} \quad (26)$$

where τ_a is a reference stress $T_c = Q/n R$ and α is the real contact area and $\tau_0 = \alpha \tau$. Here T_c is an absolute temperature (in $^\circ\text{K}$). The term T_i has been added to the denominator, because in the following section T is the background temperature rise with respect to the initial temperature (in the case of the experiments this will be the room temperature $T = 293^\circ\text{K}$).

4.4 Local and background temperatures

The growth of α with temperature (due to thermal weakening of σ_c) may reduce or even surpass the weakening due to the right-hand term in (26), which may explain the results that no significant weakening is observed under low slip rate even at high temperatures (Noda et al., 2009; King & Marone, 2012).

However, the growth of the contact area is controlled mainly by formation of new asperity contacts (as opposed to growth of pre-existing ones, (Persson, 2000)) and involves a sensibly deeper rooted strain in a larger volume than the immediate layer below asperity contact. Consequently the increase of α should be sensitive to the average increase of the interface temperature, or background temperature T , while the weakening of τ_y will be sensitive to the local, transient temperature peak $T + \Delta T$ reached at the asperity contact, where ΔT is the transient temperature increase in the asperity (Fig. 2-b). Provided that the slip rate is high, frictional heat has little time to diffuse away from the asperity during its limited contact lifetime,

therefore the excess temperature ΔT will be significant (Archard, 1959; J. R. Rice, 2006). However with continued slip the local overheating ΔT starts diffuse away from the asperities and gradually contribute to the rise the background temperature T .

If the background temperature continues to rise (Fig. 2-c) at some point the formation of a pervasive layer of amorphous material, melt, wear product or viscous nanocrystalline material may fill the interstitial space between asperities, as a saturation value of $\alpha \approx 1$ is reached. In case of a continuous lubricant layer, under high velocity the thermal gradient in the vicinity of the slip zone is very steep and an extremely thin ($< 100 \mu\text{m}$), overheated and low effective viscosity layer develops (Fig. 2-c). This situation has been documented in the case of frictional melt (Nielsen et al., 2008) and in the case of coseismic viscous flow in coseismic ultramylonites (Pozzi et al., 2019).

Consequently, we may consider that under high slip velocity, the growth of α is initially negligible (i.e., models of flash weakening acting in the very early stages of slip), but gradually increases with the accompanying growth of a pervasive lubricant layer, in which case the lubricant effect will compensate the increase in contact area and the friction will not increase.

However, the transition from an initial flash heating to a fully developed lubricant layer can be complex and non monotonous, especially at low normal stress. A relative restrengthening can occur due to the increase of the contact area ratio α with temperature rise, and the straining and elongation of the contact asperities, while voids are filled by products of comminution, decomposition or cool melt. Microstructures corresponding to such stages were described to some extent for experiments on Gabbro under increasing slip amounts, see Hirose and Shimamoto (2005).

5 Signature of thermal weakening in the experimental data

5.1 Weakening and temperature change

The particular scaling of weakening with friction, slip velocity, and frictional power systematically observed in high velocity friction experiments, is compatible with a thermal signature. If temperature is the culprit, weakening should be achieved after a slip distance scaling as $u_c \propto 1/(\tau^2 V)$ and after slip duration scaling as $t_c \propto 1/(\tau V)^2$, as argued in Nielsen et al. (2010). Indeed for an indicative constant value of shear stress and slip rate, an indicative solution of (7) with constant τV yields a temperature rise $T_c = \gamma \tau_c V \sqrt{t_c}$ after a time inter-

val t_c , and solving for time yields $t_c = T_c^2 / (\gamma \tau V)^2$. Replacing for slip $u_c = t_c V$ we obtain $u_c = T_c^2 / (\gamma^2 \tau^2 V)$.

To illustrate this we may compare two similar experiments conducted on marble in Fig. (3-a,b), where average frictional power $\overline{\tau V}$ differs by about a factor of two, and average $\overline{\tau^2 V}$ by a factor of six. An similar drop to 1/3 of the initial shear stress is achieved in the two experiments at slip distances which differ of about a factor of six. Similarly, the experiments indicate that weakening time t_c scales roughly as the inverse power squared $(\tau V)^2$ as predicted.

An upper bound temperature can be obtained using equation (7) with no heat sinks, and $\rho = 2700.0 \text{ kg/m}^3$, $c = 833 \text{ J/K}$ and $\kappa = 0.821 \cdot 10^{-6} \text{ m}^2/\text{s}$, for mass density, heat capacity and thermal diffusivity of marble, respectively (Merriman et al., 2018). The estimated T curves are represented in Fig. (3), showing that a comparable temperature rise ($T \approx 190^\circ \text{ C}$) is achieved in both experiments at an equivalent weakening stage. These simple scaling relations seem to reinforce the idea that background temperature T exerts a strong control on the weakening.

However, at a time where weakening is already pronounced, the background temperature is still much too low ($T \approx 210^\circ \text{ C}$) to trigger melting or decomposition processes (a lower bound $\approx 570^\circ \text{ C}$ is indicative of calcite decomposition). A similar observation can be made for weakening of gabbro (Figure 4), with the example of experiment s555 where pervasive frictional melt formed at advanced stages ($t > 1 \text{ s}$). Substantial weakening is observed much earlier ($t \approx 0.15 \text{ s}$). Using $\rho = 3000 \text{ kg/m}^3$, $c = 715 \text{ J/K}$ and $\kappa = 1.1 \cdot 10^{-6} \text{ m}^2/\text{s}$ for gabbro (Miao et al., 2014), the background temperature estimate is still only $\approx 200^\circ \text{ C}$ after weakening to 1/3 of peak. The expected bulk melting temperature, about 1200° C , is achieved only later in the experiment.

Efficient weakening occurs at consistently lower background estimated temperatures than those expected to induce weakening of the material through decomposition or melting. However local intensification of heating ΔT well above that of the background temperature T can be achieved if stress is concentrated on a fraction of the contact area only. This concentration mechanism forms the basis of the asperity flash heating (Archard, 1959; J. R. Rice, 2006), one of the frictional models discussed and tested below. In the coming sections we will define T and ΔT and demonstrate that both are of fundamental importance in the weakening process.

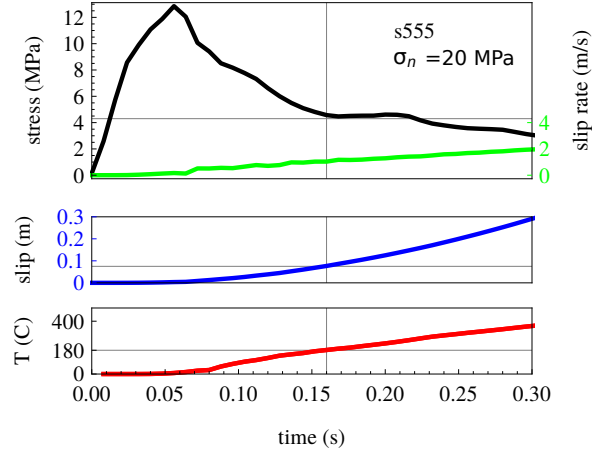


Figure 4. Evolution of stress and estimated temperature for experiment s555 performed on gabbro at 20 MPa normal stress. Weakening is initiated at ≈ 0.05 s. In this experiment, pervasive melt is observed about 1s after slip initiation; however consistent weakening (drop to 1/3 of peak stress) precedes the onset of pervasive melt, and under estimated background temperatures (ca. 200°C) well below the melting point (ca. 1200°C).

5.2 Weakening of Nitrogen-cooled marble

In Fig. (5-a) we compare two experiments s876 and s880, performed on solid calcite (Carrara marble) under identical conditions, except that in s880 the rock sample was immersed in liquid Nitrogen for several seconds immediately before the experiment. This is a simple experimental test to verify that the background temperature difference has an effect in line with prediction of basic dimensional analysis of thermal weakening. Alternatively the temperature of the sample may have been raised before the experiment, but cooling poses lesser technical difficulties.

We estimate that the initial temperature of the sample dropped to $\approx -100^\circ$ C within a few millimeters of surface, i.e., at a temperature 120°C lower than the initial (ambient) temperature for s876. If background temperature plays a role in the weakening, we expect to see some delay in the weakening for s880, which we may estimate as follows. Let T_c be the temperature rise achieved in s876 after sliding for about $t = 0.19$ s (at which point the stress dropped at 1/3 of the peak). Reasoning along similar lines as in the previous section we have $T_c = \gamma \tau V \sqrt{t}$. For s880, assuming that a similar temperature rise is reached after sliding t' seconds, then $T_c = -120 + \gamma \tau' V' \sqrt{t'}$. Taking indicative values $\tau \approx 3$ MPa, $\tau' \approx 3.3$ MPa, $V \approx 0.65$ m/s, $V' \approx 0.9$ m/s during the weakening interval, computing γ with the same parameters for marble as

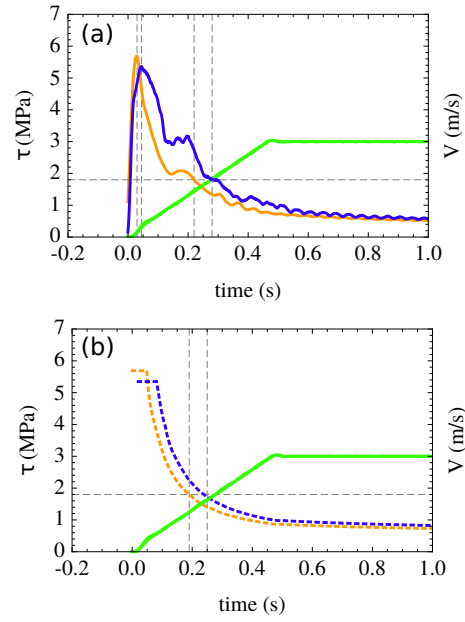


Figure 5. Weakening curves for experiments s876 and s880, performed under identical conditions (normal stress 10MPa, target velocity 3 m/s, acceleration 6.5 m/s^2) except that s880 was previously cooled with liquid Nitrogen to a temperature of about -100° C . (a) Experimental data. (b) Numerical simulation based on FWSS model. A delay of about 0.05 s is observed in both the experiment and the model.

in the previous section, and equating T_c for both experiments, we obtain $t' = (\sqrt{t}\tau V/(\tau'V') + 200/(\gamma\tau V))^2 = 0.24$ s, and a delay $t - t' \approx 0.05$ s, which is roughly the delay observed in the experiment. A more accurate computation of the weakening, including the full evolution of T is shown in figure (5-b), yielding similar delay times (the details of the full model developed in further sections).

6 Test of thermal weakening models

We test the fit of experimental with two thermal weakening models: a direct Arrhenius thermal dependence, and a model flash weakening (Rice 2006) which includes both the evolving background temperature and heat sources and sinks. We discuss the differences between flash weakening and frictional of melting, and test both thermal weakening models for either.

Two end-member lithologies were tested here, a calcite build rock (Carrara marble) and a silicate build rock (microcrystalline gabbro). These show quite different behaviour under frictional heating, as gabbro will undergo profuse melting past the initial stages of slip, but not the marble. Therefore the micromechanics of friction are similar in the initial part of slip, but differ more widely in the later phases in particular the recovery during the deceleration phase. The flash weakening law reproduces reasonably well the recovery in marble, but it over-predicts the recovery in gabbro. Recovery of marble has been considered in the context of thermal-dependent, diffusion creep plasticity Violay et al. (2019). Recovery of gabbro has been analysed in a full model of frictional melting (Nielsen, Mosca, et al., 2010), but we propose here a simplified alternative model which follows an Arrhenius thermal dependence on background temperature.

All numerical replications of the experiments are performed by imposing the experimental slip velocity history and the peak stress (i.e. static friction coefficient times normal stress). The temperature is revised at each time step based on the shear heating power as a heat source, and both thermal diffusion and dissipative heat sinks. (Considering that the friction model should be predictive, the heat source is based on the computed shear stress, not the experimentally measured shear stress).

Rock properties (κ, c, ρ) are fixed for a given lithology (see Table 1). Friction laws are based on either two or three parameters, as indicated in the text and the figures. For the solution of temperature diffusion, we including heat sinks due to endothermal phase transitions

Rock type	κ (m ² s)	ρ (kg m ⁻³)	c (J K ⁻¹)
Carrara Marble	0.82 10 ⁻⁶	2700	713
Gabbro	1.1 10 ⁻⁶	3000	715

Table 1. Rock parameters used throughout the paper (κ, ρ, c are thermal diffusivity, mass density and heat capacity, respectively).

which follow (6). By trial and error we find optimal combination of frictional parameters and heat sink parameters T_s, C_s to fit the mechanical data (friction) of each lithology.

6.1 Background temperature only - Arrhenius dependence

From the discussion and the examples of 5.1 it is clear that (1) weakening precedes any substantial rise of background temperature, however (2) the background temperature still plays an important role in the weakening. We first ask the question of how a direct temperature dependence alone is capable of fitting the data where T is the background temperature.

Using eq. (26), a straightforward Arrhenius dependence for the shear stress requires adjustment of two parameters T_c and τ_0 . Two additional parameters T_s, C_s are introduced to account for heat sinks (eq. 6) due to endothermal phase transitions. The shear value τ used in the model is the smaller of either that obtained from eq. (26) with the current temperature value, or that of the peak stress $\tau_p = \mu_f \sigma_n$ (where μ_f is static friction coefficient and σ_n is normal stress).

(1) Case of melting. Parameters used for the Arrhenius thermal weakening law (eq. 26) are $T_c = 2700$ °K and $\tau_0 = 7 \cdot 10^4$ MPa. The parameters used for the heat sink (eq. 6) are $C_s = 40 \cdot 10^6$ J s⁻¹m⁻² and $T_s = 2000$ °C. We note that a strong trade-off exists between τ_0 and T_c in the Arrhenius dependence, whereby increasing τ_c can be compensated by lowering T_c to achieve a very similar result, therefore such values are purely indicative. The same remark applies to the trade-off between C_s and T_s .

Equation (26) with a single mechanism captures some essential features of fast-slip weakening. However to accurately capture both the very initial weakening and the recovery phase,

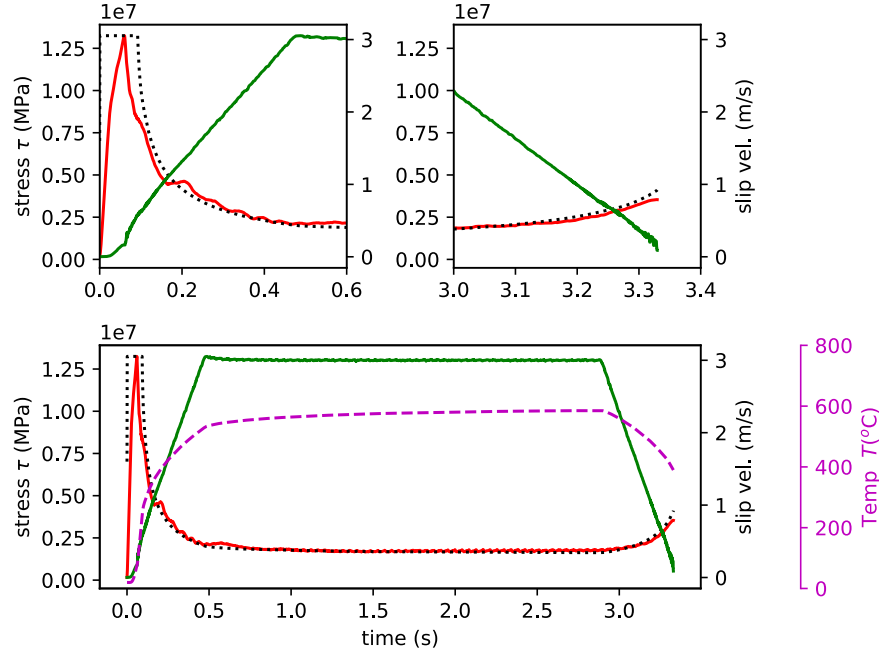


Figure 6. Experimental fit of gabbro friction with Arrhenius thermal weakening and heat sinks (normal stress 20 MPa). Solid red: measured experimental shear stress. Dotted black: model friction. Solid green: measured slip velocity. Dashed purple: computed temperature.

a combination of strong thermal dependence and large heat sink need to be included, to the point that the background temperature rise remains unrealistically low. This suggests that a simple model of viscous shear heating is not a realistic description of the microscale process. Alternatively, in the case of melting, the heat sink q_s would implicitly incorporate the effect of heat removal by extrusion, which is not accounted for explicitly in this model –as further discussed in section (6.3)–. The effect is that the computed temperature T be biased toward lower values.

(2) Case of no melting. We now use the same Arrhenius weakening model but in an attempt to reproduce the case of Carrara marble. A similar approach was adopted in Violay et al. (2019) where plastic deformation of calcite within a thin layer was assumed to follow an Arrhenius-like thermal dependence. In Pozzi et al. (2019) the steady-state friction in calcite was also interpreted in similar terms, and microstructural evidence of plastic flow were provided in support of this high-velocity deformation process. Parameters used for the Arrhenius thermal weakening law (eq. 26) are $T_c = 2000$ °K and $\tau_o = 3 \cdot 10^4$ MPa. The parameters used

for the heat sink (eq. 6) are $C_s = 50 \cdot 10^6 \text{ J s}^{-1} \text{ m}^{-2}$ and $T_s = 2000 \text{ }^\circ\text{C}$. As seen in Supplementary Materials (Fig. S1) the recovery of friction during the deceleration is severely underestimated, in addition, the temperature again is unrealistically low.

While the Arrhenius dependence is capable of reproducing the main features of frictional melting, it is more problematic to use it in the case of marble where no melting occurs. This is not altogether surprising, as the Arrhenius model assumes the shearing of a layer with temperature dependent viscosity, a situation well adapted to frictional melting. However, in the case of marble, a model of flash weakening is likely to occur in the initial part of the slip, before the development of a continuous, high-temperature layer of material.

6.2 Flash weakening with background temperature evolution, heat sources and sinks (FWSS)

We explore here a model of flash weakening with sources and sinks (FWSS) of heat included in the temperature estimation. Flash weakening and heating of contact asperities has been proposed as a model for high velocity friction evolution (Archard, 1959; J. R. Rice, 2006; Rempel & Weaver, 2008; Beeler et al., 2008). There are strong experimental indications (Goldsby & Tullis, 2011; Violay et al., 2011; Tisato et al., 2012; Violay, Nielsen, Gibert, et al., 2013; Violay, Nielsen, Spagnuolo, et al., 2013; Violay et al., 2014, 2015; Chen & Rempel, 2014; Acosta et al., 2018) that this model is relevant for high velocity experiments, in both silicate- and carbonate-built rocks, at least in the first millimeters of slip or until melting or decomposition of the rock minerals creates an almost continuous, amorphous interstitial layer. One motivation to explore flash heating is that weakening precedes the substantial rise of the background temperature of the sliding interface (as discussed above in connection to figures 3 and 4). Initial thermal weakening may be achieved only if local temperatures $T + \Delta T$ at asperity contacts are much higher than the background temperature T .

The FW model considers that the lifetime of asperity of linear dimension D is indicatively $t_c = D/V$. For an asperity sheared under incipient yield stress τ_c , the heating results from frictional power $\tau_c V$. Assuming that heat diffusion is mostly perpendicular to the fault, during the asperity lifetime, solution of (7) with $q \approx \tau_c V = \text{const.}$ yields the local temperature rise $\Delta T = \gamma \tau_c V \sqrt{t_c} = \gamma \tau_c \sqrt{V D}$, and the time during contact at which the asperity weakens is $t_w = (T_w - T)^2 / (\gamma \tau_c V)^2$. Upon defining a threshold temperature $T_w = T + \Delta T$, a minimum slip rate V_w can be computed at which shear resistance is lost within the duration of an asper-

ity contact lifetime:

$$\begin{aligned} V_w &= \frac{1}{\gamma^2 \tau_c^2 D} \text{Max}[T_w - T, 0]^2 \\ &= B \text{Max}[T_w - T, 0]^2 \end{aligned} \quad (27)$$

The average strength of an asperity contact during its lifetime will be $\tau_a = (\tau_r(t_c - t_w) + \tau_c t_w)/t_c$, where τ_r is the residual shear stress supported by the weakened asperity. Assuming an asperity population with dominant dimension D , using $\tau_p = \alpha \tau_c$, $\tau_w = \alpha \tau_w$, $\tau = \alpha \tau_a$ and noting that $t_w/t_c = \tau_c (T_w - T)^2 / (\gamma^2 \tau_c^2 V D) = \tau_c V_w / V$ it is found (J. R. Rice, 2006; Rempel & Weaver, 2008; Beeler et al., 2008) that the effective sliding shear stress is:

$$\tau \approx (\tau_p - \tau_w) \left(\frac{V_w}{V} \right) + \tau_w \quad (28)$$

for $V > V_w$. The flash weakening friction is adjusted with the three parameters B ($^{\circ}\text{C}^{-2} \text{ m s}^{-1}$), T_w ($^{\circ}\text{C}$) and τ_w (Pa). The shear value τ used in the model is the smaller of either that obtained from eq. (27-28) with the current temperature value, or that of the peak stress $\tau_p = \mu_f \sigma_n$.

In previous models, the variation of the background temperature T is often neglected in (27), with the consequence that V_w remains constant (Noda et al., 2009; Goldsby & Tullis, 2011). Indeed the direct numerical computation of T with classical methods can be rather costly and inefficient. However T increases substantially after the first millimeters of slip as shown in figure (3), and unless evolution of T is included, flash weakening fails to reproduce accurately the friction recovery observed in the experiments. One immediate evidence that friction is not purely velocity-dependent is the lack of symmetry in the acceleration and deceleration phase, whereby an hysteresis loop is observed –see for example the τ vs. V representation in Figure (8-d), and also experiments reported in previous studies (Goldsby & Tullis, 2011; Proctor et al., 2014). Thus inclusion of background temperature, which is substantially higher in the recovery phase than in the weakening phase, allows to moderate the velocity effect by acting as a state variable. In addition, we note that an accurate evolution of T should include both heat sources (frictional power τV) and any significant heat sink (other than diffusion).

Indeed this is important to obtain an hysteresis cycle where initial weakening and the final recovery are not symmetrical, and are not purely velocity dependent. The higher temperature at the end of experiment allows the friction recovery to be relatively slower, as observed. However if the heat sinks are excluded, the final temperature will be too large and the recovery will be underestimated.

Therefore, only the inclusion of background temperature evolution due to both sinks and sources allows an accurate reproduction of the experiments including the recovery phase. The FWSS law is based on the full set of equations: (3, 7, 27, 28); the only input variable is the slip velocity $V(t)$. Input parameters are (1) the group $\gamma^2 \tau_c^2 D$ (with dimensions $[L T^{-1}]$, allowing the definition of a characteristic velocity V_w), (2) the peak stress τ_p (which may be predicted using $\tau_p = \mu \sigma_n$) and residual stress τ_w (for computation of τ) and (3) C and T_s (for a single dominant heat sink).

One of the peculiarities of the model described by equations (28) is the absence of explicit dependence on normal stress. However, taking into account the evolution of background temperature T , with τV as a heat source implicitly includes normal stress. Indeed during the initial part of the slip $\tau = \tau_p = \mu_s \sigma_n$ where μ_s is the initial friction coefficient (of the order of 0.6 before onset of weakening), so the heat production rate is higher if the normal stress is higher. On the other hand, if the initial (peak) stress is higher under higher normal stress, temperature rise and weakening will be accelerated by a similar proportion. As a consequence, the weakening slip distance and the fracture energy may not be significantly altered by a change in normal stress. This behavior was indeed observed in a synthesis of different high velocity friction laboratory experiments Nielsen, Spagnuolo, Violay, et al. (2016); Nielsen, Spagnuolo, Smith, et al. (2016).

In figures (7–10) we compare the FWSS model to experiments performed on samples of solid carbonate (carrara marble). Notably, the shear stress curves in the weakening, steady-state and recovery phases are reasonably well matched with the same set of parameters although the three experiments are different in terms of loading conditions (normal stress and target slip rate).

An interesting test of the robustness of the model, is whether the outcome of different experimental conditions (normal stress, slip velocity) can be reproduced with a single set of parameters.

We show the result in four different experiments in Figures (7–10), and in most cases the weakening, steady-state and recovery are all reasonably well reproduced with a single set of parameters. The parameters for flash weakening (eq. 27 and 28) are $T_w = 800^\circ\text{C}$, $t_w = 0.5 \cdot 10^6 \text{ Pa}$, $B = 0.7 \cdot 10^{-6} \text{ }^\circ\text{C}^{-2} \text{ m s}^{-1}$. The parameters used for the heat sink (eq. 6) are $C_s = 3 \cdot 10^6 \text{ J s}^{-1} \text{ m}^{-2}$ and $T_s = 2000 \text{ }^\circ\text{C}$. One exception, though, is experiment s324 which was performed under the most extreme frictional work rate (highest normal stress and slip veloc-

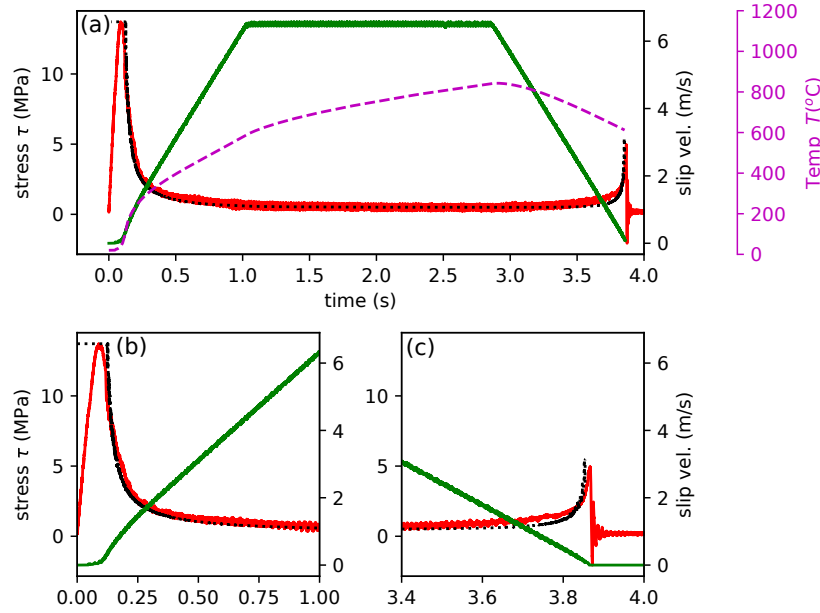


Figure 7. Experiment s308 on Carrara marble, data and model (normal stress 20MPa, target velocity 6.5 m/s, acceleration 6.5 m/s^2). Shear stress in experiment (red) and in model FWSS (black dashed); imposed slip velocity (green). Temperature evolution (modeled) including heat sinks (purple dashed). (a) is whole experiment and (b-c) are zoom of start and end. For marble, parameters of rock, FWSS and heat sinks are indicated in text.

ity combination). In this case the heat sink parameter C_s has to be doubled to reproduce correctly the recovery. One possible interpretation is an additional heat sink due to abundant loss by radiation is substantial in this experiment, due to the relative large heat production and higher temperatures.

6.3 Flash weakening followed by the formation of a viscous shear layer

A model for frictional melting has been proposed for both the steady-state (Nielsen et al., 2008) and the transient (Nielsen, Mosca, et al., 2010) behaviour. It accounts for the advancement of a melting boundary (solution of a Stefan problem) and the possibility that melt extrusion occurs through lateral injection veins (natural faults, Di Toro et al. (2005)) or at the edges of the sample (experimental simulated faults Niemeijer et al. (2009); Violay et al. (2014)). We will only revisit some features of such model here, and test to what extent a simpler flash weakening model differs from the melting dynamics.

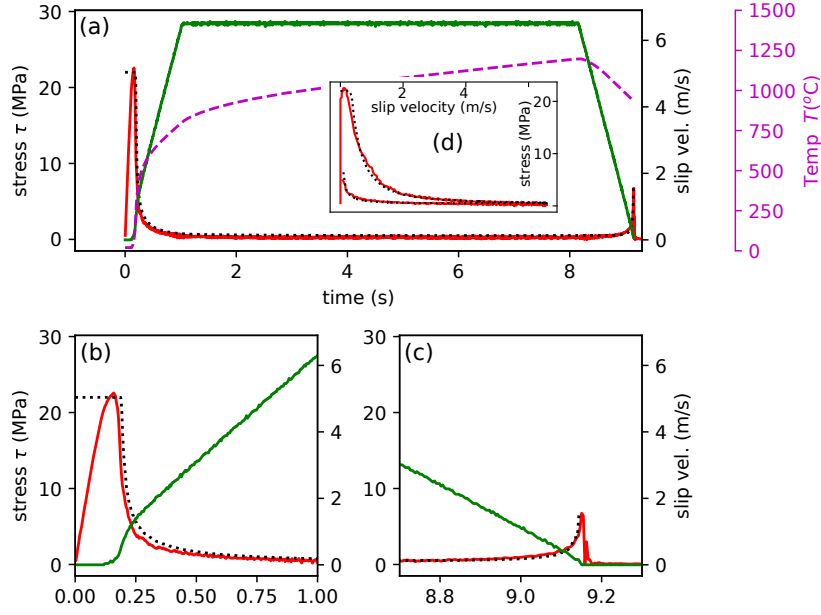


Figure 8. Experiment s324 on Carrara marble, data and model (normal stress 30MPa, target velocity 6.5 m/s, acceleration 6.5 m/s^2). Same parameters as in figure 7 (except for the heat sink which was changed to $C_s = 6 \cdot 10^6 \text{ J s}^{-1} \text{ m}^{-2}$ instead of $3 \cdot 10^6$). (a-c) Show variables as a function of time, (d) shows stress versus velocity.

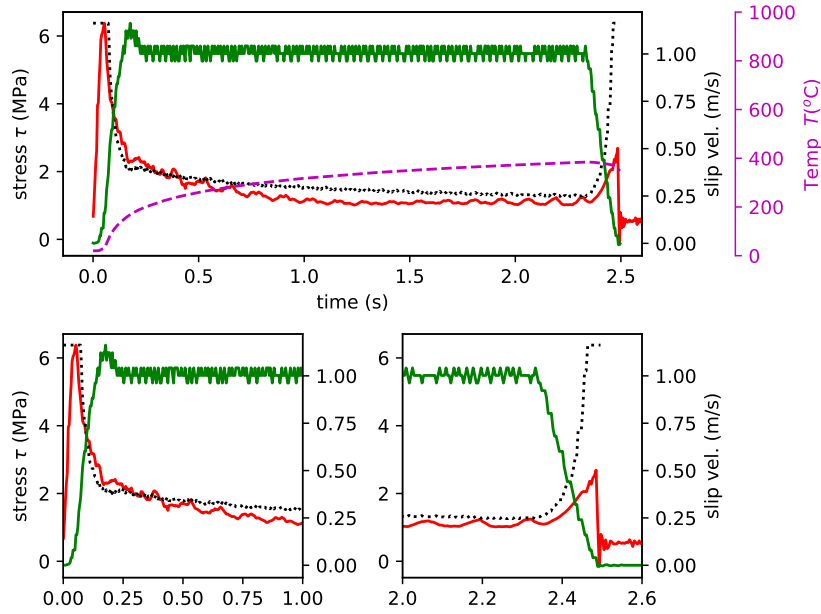


Figure 9. Experiment s257 on Carrara marble, data and model (normal stress 10MPa, target velocity 3 m/s, acceleration 3 m/s^2). Same parameters as in figure 7.

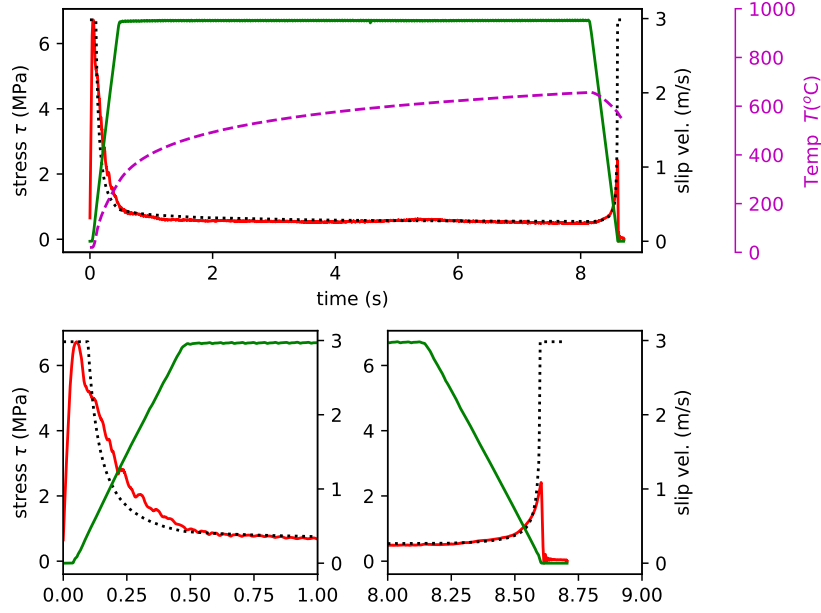


Figure 10. Experiment s330 on Carrara marble, data and model (normal stress 10MPa, target velocity 3 m/s, acceleration 6.5 m/s^2). Same parameters as in figure 7.

In the case of frictional melt with extrusion, the thermal balance is quite different from that resulting in (2) from simple diffusive temperature. Apart from the heat loss due to phase transitions already discussed above, there is a radical change in the thermal diffusion equation with an additional convective term as a consequence of the advancement of the melting front into the rock:

$$\partial_t T = \kappa \partial_z^2 T + v \partial_z T + \frac{\delta(z) q}{\rho c}. \quad (29)$$

where v is the current velocity at which the melt boundary is advancing into the solid. Heat sinks due to phase transitions in this case are essentially due to melting latent heat L such that $q_s = v \rho L$. Thermal diffusion solutions with a moving boundary are known as Stefan's problem. It can be assumed that the boundary between melt and solid rock is at the melting temperature T_m . As a consequence v can be computed by applying the boundary condition that $T = T_m$ and $\partial_t T = 0$ at the melting boundary ($x = 0$). A method to integrate the numerical computation of v into an efficient, discrete time-stepping scheme is detailed in section (8).

One key process in the presence of melting and extrusion is the advancement of the melting front which counteracts the advancement of the thermal diffusion. In the absence of melting and extrusion, as in the case of flash weakening, the background temperature T is representative of recent frictional power dissipated on the fault, which induces heating within a finite thickness around the slip zone. Therefore temperature may be considered as a state variable storing the memory of the frictional heating history. However, advancement of a melting front combined with extrusion will constantly reset the heat stored around the slip zone. The boundary will remain at the melting temperature $T \approx T_m$. Super-heating above T_m may occur within the melt reaching a maximum at the centre of the melt layer (Nielsen et al., 2008), but melt is rapidly extruded. Heat diffusion penetrates to an indicative depth $z = 2\sqrt{\kappa t_r}$ within a given time interval t_r . Given a shortening rate v (melt front advancement) the typical time of residence of the heat in the rock adjacent to the slip zone will be $t_r = z/v$ resulting in $t_r = 4\kappa/v^2$ upon substitution of z . Therefore the thermal memory of the system is reset over times of the order of t_r , i.e., a few seconds, assuming shortening rates of 1 mm/s and standard diffusivity values.

As discussed in section (5.1) and in Fig (4), it appears that weakening predates the bulk melting temperature. Therefore it can be assumed that the initial part of the weakening, before pervasive melt starts, is due to flash weakening behaviour and can be modelled as such.

At later times, when pervasive melt and extrusion occur, a full steady-state condition may be reached, as predicted by the model of Nielsen et al. (2008) and experimentally confirmed by Violay et al. (2014). This situation is not completely retrieved through the heat sinks described by equation (2). The buffering term q_s in (2) represents heat sinks which inhibit the temperature rise, but which are not as efficient in achieving rapidly a full steady-state. The boundary migration needs to be included explicitly for an accurate temperature evolution; however temperature diffusion in the presence of heat sinks does allow reproduce to a certain extent the appearance of a steady-state solution, because the background temperature reaches a plateau although the temperature diffusion continues to progress.

Finally, we note that the frictional recovery during the deceleration phase is expected to differ between flash weakening and frictional melt, although in both cases the sliding surface has undergone an irreversible transformation, and the background temperature is higher.

Ideally, in the occurrence of melting, a mixed model should be used with a transition from flash heating to frictional melting after the background temperature reaches T_m . Such a

transition can be rather complex, and several experiments show that there is a partial frictional recovery at that stage (Hirose & Shimamoto, 2005), although it is hardly found at higher normal stress (Hung et al., 2019).

Leaving the implementation of the mixed flash heating/ frictional melting model for future work, instead we show in Figure (6) a fit with Arrhenius dependence, which is discussed in section (6.1). In addition, we tested the flash weakening law of section(6.2) as an approximation where melting occurs. We find that with flash weakening alone does not predict the recovery accurately in the presence of melting. An example is shown in Supplementary Material (Figure S2).

A mixed model can be developed also in the case of calcite, where an initial flash-weakening process is followed by the formation of a continuous viscous layer which undergoes high velocity plastic shear, as posited in in Violay et al. (2019) for bare surfaces in frictional contact. Where the slip initiates within a gouge, the eventual formation of a viscous layer after several mm of slip is also observed by Pozzi et al. (2019), however, the initial weakening includes a slip hardening phase. A microstructural evolution with complex processes is observed, before the viscous shear is mature. This process is arguably difficult to represent with a flash weakening model.

Finally, a mixed model would also be indicated in the case where fluids are initially permeating the fault surface allow for elasto-hydrodynamic weakening: as slip accelerates, a transition between three lubrication regimes (boundary, mixed, and fully lubricated regimes) will occur as discussed in Cornelio et al. (2019).

7 Regularisation for use in dynamic rupture modelling

In dynamic rupture models the slip velocity history is a result of the computation, it is not imposed and not known a-priori. Thus the frictional form (28) with its strong rate-dependence may generate very abrupt and fast and fast weakening, resulting in under-sampling of the rupture front by the numerical scheme, and the consequent artefacts in the results. A similar situation arises in the ill-posed problem of rupture at bi-material interfaces, where a contracting slip pulse rapidly becomes under-sampled (rupture, 1997).

This problem can be circumvented by introducing a regularised shear stress value τ_{reg} which obeys a time-dependent evolution law. Let τ be the target value of shear stress at time t , which is obtained by implementing a law (such as flash weakening described in section 6).

We can write a regularized form of shear stress τ_{reg} by adding a time-evolution law on top of the instantaneous value of friction such that:

$$\frac{\partial \tau_{reg}}{\partial t} = \frac{\tau - \tau_{reg}}{t_a} \quad (30)$$

which by the usual 1st order backward Euler scheme result in the discrete form:

$$\tau_{reg} = \frac{\tau_{reg}^- + \frac{\delta t}{t_a} \tau}{1 + \frac{\delta t}{t_a}} \quad (31)$$

where τ_{reg}^- is the value at the previous time step.

Thus t_a can be fixed to the lowest limit compatible with the numerical grid, producing a regularised (smoothed) solution. In principle, with sufficient computing resources the numerical grid spacing and t_a may be reduced until τ and τ_{reg} converge.

8 Conclusions

We demonstrate that the background temperature is paramount in accounting for the high-velocity friction. However computation of temperature diffusion can result in a numerically costly computation, in particular for models of an extended fault surface where T needs to be tracked at a great number of points. Therefore we design an efficient and accurate method based on wavenumber transform and a small number of memory variables (less than 32 variables fit the analytical solution within 1/10000). Inclusion of thermal dependence of diffusivity and heat capacity is straightforward in the scheme, with a minimum additional computation. It is also straightforward to include heat sinks.

We proceed to test friction models based on a thermal weakening where the background temperature accounts for heat sources and heat sinks including diffusion and decomposition. The model including a simple Arrhenius dependence on background temperature captures some of the main features of the weakening, however fails to account for the initial rapid weakening. A flash weakening model, instead, captures well the initial weakening, however it requires to include the evolution of the background temperature to reasonably reproduce friction from start to end. An accurate background temperature is obtained by including diffusion but also other heat sinks which buffer the maximum temperature rise and allow to create an apparent steady-state.

We discuss the differences between flash weakening and profuse frictional melting, and we conclude that both can take place within a single slip episode, with the flash heating occurring at the start. Despite this, we show that flash weakening model including thermal de-

pendence with heat sources and sinks is able to reproduce cases of frictional melting reasonably well over the limited interval of parameters of the experiments shown here in support. However, while high velocity friction in silica built rocks has been modelled either with flash weakening or frictional melting, we argue that a more accurate representation should include both, with the transition from flash weakening to frictional melting, an endeavour that we leave for future work.

Finally, the experiments presented here are limited to precut, cohesive rocks of two end-members (carrara marble, gabbro) under dry conditions. One needs consider that rupture on natural faults will develop in different lithologies, including clays, and in more complex ways, including diffuse strain, processes such as gradual slip localisation in fault gouge, multiple branching of rupture and other dissipative processes taking place off-fault. These process take place in a volume rather than on a planar surface of limited gouge thickness. They interact and contribute to the energy balance generating a stress-strain relation which translation into an equivalent frictional slip remains an open problem. Until then, such limitations need to be kept in mind when using laboratory derived friction laws in earthquake models.

Looking further, the efficient method developed here to compute the diffusive response to a boundary heating problem, may be directly implemented to solve other cases where the diffusion equation applies, which are many and diverse (e.g. fluid diffusion across porous media, chemical diffusion across a membrane, erosional processes, photon diffusion in scattering media, financial mathematics, etc...). The efficient computation proposed here for heat diffusion can be redesigned as a boundary condition with constant temperature, or to simulate an infinite, homogeneous medium at the edges of a numerical model. In the form presented here only the diffusion in 1D, perpendicular to the boundary is considered. Future studies may explore an extension to multiple dimensions, to develop a diffusion equivalent of the Perfect Matching Layer method proposed for elastic waves (Collino & Tsogka, 2001; Festa & Nielsen, 2003).

Appendix I: Temperature solution in the presence of melt boundary migration (Stefan problem)

We repeat the above wavenumber solution in the case where a convection term is present, for example, due to the shortening of the sample occurring due to melting boundary migration combined with the extrusion of the melt (see Stefan problem solution in Nielsen et al. 2008, Nielsen et al. 2010). Assume that the boundary is migrating into the solid at a velocity v in

direction z , and that in our referential z is attached to the boundary. In such case the heat diffusion equation may be written with an additional term accounting for mass transport at velocity v equal and opposite to the boundary migration velocity:

$$\partial_t T = \kappa \partial_z^2 T + v \partial_x T + \frac{\delta(z)}{\rho c} \frac{q}{c}, \quad (32)$$

which, in the wavenumber domain yields:

$$\partial_t \theta = -(\kappa s^2 + v s) \theta + \frac{q}{\rho c}. \quad (33)$$

(Note that here z is the distance from the melting boundary, in the Eulerian referential not attached to the flow of particles). The only difference with the previous solution is the replacement $\kappa s \rightarrow (\kappa s^2 + v s)$ so that we may write

$$T(z=0, t) = \frac{2}{\pi \rho c} \int_0^t dt' \int_0^\infty ds q(t') e^{-(\kappa s^2 + v s)(t-t')} \quad (34)$$

and solving for the inner integral we obtain:

$$T = \frac{1}{\rho c \sqrt{\pi \kappa}} \int_0^t dt' \frac{q(t')}{\sqrt{t-t'}} f_a(t-t') \quad (35)$$

where (36)

$$f_a(t) = e^{\frac{v^2 t}{4\kappa}} \text{Erfc} \left(v(t) \sqrt{\frac{t}{4\kappa}} \right) \quad (37)$$

688 Interestingly, we remark that the solution is in all points similar to the previous, except for the
 689 multiplication by function $f_a(t)$ which behaves essentially like a memory-fading term with a
 690 characteristic time of about $t_c = 4\kappa/v^2$ (making the approximation that $v \approx \text{Const}$. Quite in-
 691 tuitively, t_c is the average time of residence of heat inside the solid before it is erased by the
 692 shortening process. Indeed, if we write the penetration depth for diffusion during an interval
 693 t_c as $z = 2\sqrt{\kappa t_c}$, and we write the advancement of the boundary as $z = v t_c$, if we equate both
 694 values of z we obtain the same value for t_c .

If a single, equivalent melting temperature T_{melt} may be defined, we note that the equality $T(z=0, t) = T_{melt}$ and $\partial_t T(z=0, t) = 0$ should be verified. However, $\partial_t T$ can be expressed through the inverse Fourier transform such as:

$$\partial_t T(z=0) = \frac{2}{\pi} \int_0^\infty \partial_t \theta ds = 0 \quad (38)$$

and inserting 33 into 38, we obtain at the melting boundary the equality

$$-\int_0^\infty \kappa s^2 \theta ds - \int_0^\infty v s \theta ds + \int_0^\infty \frac{q}{\rho c} ds = 0.$$

695 Considering that v is independent of s we can isolate it such that:

$$v = \frac{\int_0^\infty \frac{q}{\rho c} ds - \int_0^\infty \kappa s^2 \theta ds}{\int_0^\infty s \theta ds} \quad (39)$$

Discretising (39) we may solve for the melt boundary velocity v , at each time step:

$$v = \frac{\frac{M}{\rho c} \frac{q}{c} - \sum_{m=1}^M \theta_m \kappa s_m^2 \delta s}{\sum_{m=1}^M \theta_m s_m \delta s}, \quad (40)$$

696 then use the result for v in the discrete form of (34) to update the values θ_m :

$$\theta_m = \left(\frac{q(t) \delta t}{\rho c} + \theta_m^- \right) \frac{1}{1 + \delta t (\kappa s_m^2 + v s_m)}, \quad (41)$$

and, finally, compute the temperature by the inverse transform

$$T(z, t) = \frac{2}{\pi} \sum_{m=1}^M \cos(s_m z) \theta_m \delta s \quad (42)$$

697 with s_m as defined in eq. (16).

698 **Appendix II: Analytical solution of equation (10)**

Multiplying by a dummy function u we may write

$$\partial_t(u \theta) - \theta \partial_t u = -u \kappa s^2 \theta + u \frac{q}{\rho c} \quad (43)$$

699 and assume the arbitrary function u is such that both following parts of the equation are zero:

$$(u \kappa s^2 - \partial_t u) \theta = 0 \quad (44)$$

$$\partial_t(u \theta) - u \frac{q}{\rho c} = 0 \quad (45)$$

excluding the trivial solution $\theta = 0$, the first equation yields

$$u = A \exp\{\kappa s^2 t\} \quad (46)$$

replacing u into the second equation and integrating in time we obtain

$$\theta = \frac{1}{\rho c} e^{-\kappa s^2 t} \int_0^t q(t') e^{\kappa s^2 t'} dt' \quad (47)$$

$$\theta = \frac{1}{\rho c} \int_0^t q(t') e^{-\kappa s^2 (t-t')} dt' \quad (48)$$

(an extra integration constant vanishes since temperature is zero at negative times). The so-

lution for $T(x, t)$ is obtained by performing the inverse Cosine transform

$$T(x, t) = \frac{2}{\pi} \int_0^\infty \cos(s z) \theta(s, t) ds \quad (49)$$

and, at $z=0$,

$$T(0, t) = \frac{2}{\pi} \int_0^\infty \theta(s, t) ds. \quad (50)$$

Upon replacement of θ by its expression we get

$$= \frac{2}{\pi \rho c} \int_0^\infty \cos(s z) \left(\int_0^t q(t') e^{-\kappa s^2(t-t')} dt' \right) ds \quad (51)$$

$$= \frac{2}{\pi \rho c} \int_0^t dt' \int_0^\infty ds \cos(s z) q(t') e^{-\kappa s^2(t-t')} \quad (52)$$

By integrating the inner part we obtain:

$$\frac{1}{\rho c \sqrt{\pi \kappa}} \int_0^t \frac{q(t') e^{-\frac{z^2}{4\kappa(t-t')}}}{\sqrt{t-t'}} dt' \quad (53)$$

where we can check for consistency that we retrieve the classical solution of eq. (2) by setting $z=0$.

Acknowledgments

We acknowledge support by ERC CoG No. 6145705 NOFEAR. The data used in this article is available at the following public repository: <https://datahub.io/stefanazzz/thermal-weakening-2020/v/1>

References

- Acosta, M., Passelègue, F., Schubnel, A., & Violay, M. (2018). Dynamic weakening during earthquakes controlled by fluid thermodynamics. *Nat. Comm*, 9, 3074. doi: 10.1038/s41467-018-05603-9
- Andrews, D. J., & Ben-Zion, Y. (1997). Wrinkle-like slip pulse on a fault between different materials. *J. Geophys. Res.*, 102, 552-571.
- Archard, J. (1959). The temperature of rubbing surfaces. *Wear*, 2(6), 438 - 455. doi: 10.1016/0043-1648(59)90159-0
- Atkins, A., & Tabor, D. (1965, Jun). Plastic indentation in metals with cones. *Journal of the Mechanics and Physics of Solids*, 13(3), 149-164. doi: 10.1016/0022-5096(65)90018

- Beeler, N., Tullis, T., & Goldsby, D. (2008). Constitutive relationships and physical basis of fault strength due to flash heating. *J. Geophys. Res.*, *113*(B1), B01401. doi: 10.1029/2007JB004988
- Brantut, N., Han, R., Shimamoto, T., Findling, N., & Schubnel, A. (2010, Dec). Fast slip with inhibited temperature rise due to mineral dehydration: Evidence from experiments on gypsum. *Geology*, *39*(1), 59-62. doi: 10.1130/g31424.1
- Carslaw, H. S., & Jaeger, J. C. (1959). *Conduction of heat in solids*. Oxford University Press, USA.
- Chang, J. C., Lockner, D. A., & Reches, Z. (2012, Oct). Rapid acceleration leads to rapid weakening in earthquake-like laboratory experiments. *Science*, *338*(6103), 101-105. doi: 10.1126/science.1221195
- Chen, J., & Rempel, A. W. (2014). Progressive flash heating and the evolution of high-velocity rock friction. *Journal of Geophysical Research: Solid Earth*, *119*(4), 3182-3200.
- Collettini, C., Niemeijer, A., Viti, C., Smith, S. A., & Marone, C. (2011, Nov). Fault structure, frictional properties and mixed-mode fault slip behavior. *Earth Planet. Sci. Lett.*, *311*(3-4), 316-327. doi: 10.1016/j.epsl.2011.09.020
- Collino, F., & Tsogka, C. (2001). Application of the pml absorbing layer model to the linear elastodynamic problem in anisotropic heterogeneous media. *Geophysics*, *66*(1), 294-307.
- Cornelio, C., Passelègue, F. X., Spagnuolo, E., Di Toro, G., & Violay, M. (2020). Effect of fluid viscosity on fault reactivation and coseismic weakening. *Journal of Geophysical Research: Solid Earth*, *125*(1), e2019JB018883. (e2019JB018883 2019JB018883) doi: 10.1029/2019JB018883
- Cornelio, C., Spagnuolo, E., Di Toro, G., Nielsen, S., & Violay, M. (2019). Mechanical behaviour of fluid-lubricated faults. *Nat Commun*, *10*, 1274. doi: 10.1038/s41467-019-09293-9
- Cruz-Atienza, V., & Olsen, K. (2010). Supershear mach-waves expose the fault breakdown slip. *Tectonophysics*, *493*, 285-296. doi: 10.1016/j.tecto.2010.05.012,2010
- De Paola, N., Collettini, C., Faulkner, D. R., & Trippetta, F. (2008, Aug). Fault zone architecture and deformation processes within evaporitic rocks in the upper crust. *Tectonics*, *27*(4), TC4017. doi: 10.1029/2007tc002230
- Di Toro, G., Goldsby, D. L., & Tullis, T. E. (2004). Friction falls towards zero in quartz rock

- as slip velocity approaches seismic rates. *Nature*, 427, 436-439.
- Di Toro, G., Han, R., Hirose, T., De Paola, N., Nielsen, S., Mizoguchi, K., . . . Shimamoto, T. (2011). Fault lubrication during earthquakes. *Nature*, 471, 494-499. doi: 10.1038/nature09838
- Di Toro, G., Hirose, T., Nielsen, S., Pennacchioni, G., & Shimamoto, T. (2006). Natural and experimental evidence of melt lubrication of faults during earthquakes. *Science*, 311, 647-649. doi: 10.1126/science.1121012
- Di Toro, G., Nielsen, S., & Pennacchioni, G. (2005). Earthquake rupture dynamics frozen in exhumed ancient faults. *Nature*, 436, 1009-1012. doi: 10.1038/nature03910
- Dieterich, J. H. (1979). Modeling of rock friction. I: Experimental results and constitutive equations. *J. Geophys. Res.*, 84, 2161-2168.
- Festa, G., & Nielsen, S. (2003). PML absorbing boundaries. *Bull. Seismol. Soc. Am.*, 93, 891-903. doi: 10.1785/0120020098
- Fondriest, M., Smith, S. A., Candela, T., Nielsen, S. B., Mair, K., & Di Toro, G. (2013). Mirror-like faults and power dissipation during earthquakes. *Geology*, 41(11), 1175-1178. doi: 10.1130/G34641.1
- Fulton, P. M., Brodsky, E. E., Kano, Y., Mori, J., Chester, F., Ishikawa, T., . . . from Expeditions 343, 43T and KR13-08, S. (2013). Low coseismic friction on the tohoku-oki fault determined from temperature measurements. *Science*, 342(6163), 1214-1217. doi: 10.1126/science.1243641
- Goldsby, D. L., & Tullis, T. E. (2011, Oct). Flash heating leads to low frictional strength of crustal rocks at earthquake slip rates. *Science*, 334(6053), 216-218. doi: 10.1126/science.1207902
- Han, R., Shimamoto, T., Hirose, T., Ree, J.-H., & Ando, J. (2007). Ultralow friction of carbonate faults caused by thermal decomposition. *Science*, 316, 878-881. doi: 10.1126/science.1139763
- Hasegawa, A., Yoshida, K., & Okada, T. (2011, Jul). Nearly complete stress drop in the 2011 m w 9.0 off the pacific coast of tohoku earthquake. *Earth Planet Sp*, 63(7), 703-707. doi: 10.5047/eps.2011.06.007
- Hirose, T., & Shimamoto, T. (2005). Growth of molten zone as a mechanism of slip weakening of simulated faults in gabbro during frictional melting. *J. Geophys. Res.*, 110, B05202. doi: 10.1029/2004JB003207
- Hirth, G., & Beeler, N. (2015, 03). The role of fluid pressure on frictional behavior at the

- base of the seismogenic zone. *Geology*, 43(3), 223–226. doi: 10.1130/G36361.1
- Hirth, G., & Kohlstedt, D. (2004). Inside the subduction factory. In J. Eiler (Ed.), (chap. Rheology of the Upper Mantle and the Mantle Wedge: A View from the Experimentalists). American Geophysical Union, Washington, D. C. doi: 10.1029/138GM06
- Hung, C., Kuo, L., Spagnuolo, E., Wang, C., Di Toro, G., Wu, W., . . . Sieh, P.-S. (2019). Grain fragmentation and frictional melting during initial experimental deformation and implications for seismic slip at shallow depth. *Journal of Geophysical Research: Solid Earth*, 124, 11,150–11,169. doi: 10.1029/2019JB017905
- Karato, S.-I. (2008). *Deformation of earth materials: An introduction to the rheology of solid earth*. Cambridge University Press.
- King, D. S. H., & Marone, C. (2012). Frictional properties of olivine at high temperature with applications to the strength and dynamics of the oceanic lithosphere. *J. Geophys. Res.*, 117, 117, B12203.
- Lankford, J. (1996). High strain rate compression and plastic flow of ceramics. *Journal of Materials Science Letters*, 15, 445–450.
- Marone, C. (1998). Laboratory-derived friction laws and their application to seismic faulting. *Annual Review of Earth and Planetary Sciences*, 26, 643–696. doi: 10.1146/annurev.earth.26.1.643
- Merriman, J. D., Hofmeister, A. M., Roy, D. J., & Whittington, A. G. (2018). Temperature-dependent thermal transport properties of carbonate minerals and rocks. *Geosphere*, 14(4), 1961–1987.
- Miao, S., Li, H., & Chen, G. (2014). Temperature dependence of thermal diffusivity, specific heat capacity, and thermal conductivity for several types of rocks. *Journal of Thermal Analysis and Calorimetry*, 115(2), 1057–1063.
- Mitchell, T. M., Smith, S. A., Anders, M. H., Di Toro, G., Nielsen, S., Cavallo, A., & Beard, A. D. (2015, Feb). Catastrophic emplacement of giant landslides aided by thermal decomposition: Heart mountain, Wyoming. *Earth Planet. Sci. Lett.*, 411, 199–207. doi: 10.1016/j.epsl.2014.10.051
- Mizoguchi, K., Hirose, T., Shimamoto, T., & Fukuyama, E. (2007). Reconstruction of seismic faulting by high-velocity friction experiments: An example of the 1995 kobe earthquake. *Geophys. Res. Lett.*, 34, L01308. doi: 10.1029/2006GL027931
- Nielsen, S., Di Toro, G., Hirose, T., & Shimamoto, T. (2008). Frictional melt and seismic slip. *J. Geophys. Res.*, 113, B01308. doi: 10.1029/2007JB005122

- 818 Nielsen, S., Di Toro, G., & Griffith, W. A. (2010). Friction and roughness of a melting rock
819 surface. *Geophys. J. Int.*, 182, 299-310. doi: 10.1111/j.1365-246X.2010.04607.x
- 820 Nielsen, S., & Madariaga, R. (2003). On the self-healing fracture mode. *Bull. Seismol. Soc.*
821 *Am.*, 93(6), 2375-2388. doi: 10.1785/0120020090
- 822 Nielsen, S., Mosca, P., Giberti, G., Di Toro, G., Hirose, T., & Shimamoto, T. (2010). On
823 the transient behavior of frictional melt during seismic slip. *J. Geophys. Res.*, 115,
824 B10301. doi: 10.1029/2009JB007020
- 825 Nielsen, S., Spagnuolo, E., Smith, S. A. F., Violay, M., Di Toro, G., & Bistacchi, A. (2016).
826 Scaling in natural and laboratory earthquakes. *Geophysical Research Letters*, 43(4),
827 1504–1510. (2015GL067490) doi: 10.1002/2015GL067490
- 828 Nielsen, S., Spagnuolo, E., Violay, M., Smith, S., Di Toro, G., & Bistacchi, A. (2016). G:
829 Fracture energy, friction and dissipation in earthquakes. *Journal of Seismology*, 1–19.
830 doi: 10.1007/s10950-016-9560-1
- 831 Niemeijer, A., Di Toro, G., Nielsen, S., Smith, S., Griffith, W. A., Scarlato, P., ... Mariano,
832 S. (2009). A new state-of-the-art tool to investigate rock friction under extreme
833 slip velocities and accelerations: Shiva. In *Eos, trans., agu fall meeting suppl.* (Vol.
834 90(52)). (Abs. T23C-1950)
- 835 Noda, H., Dunham, E. M., & Rice, J. R. (2009, July). Earthquake ruptures with thermal
836 weakening and the operation of major faults at low overall stress levels. *J. Geophys.*
837 *Res.-solid Earth*, 114, B07302. doi: 10.1029/2008JB006143
- 838 Noda, H., Kanagawa, K., Hirose, T., & Inoue, A. (2011). Frictional experiments of dolerite
839 at intermediate slip rates with controlled temperature: Rate weakening or tempera-
840 ture weakening? *J. Geophys. Res.: Solid Earth*, 116(B7), n/a–n/a. (B07306) doi:
841 10.1029/2010JB007945
- 842 Otsuki, K., Monzawa, N., & Nagase, T. (2003). Fluidization and melting of fault gouge
843 during seismic slip: Identification in the nojima fault zone and implications for focal
844 earthquake mechanisms. *Journal of Geophysical Research: Solid Earth*, 108(B4). doi:
845 10.1029/2001JB001711
- 846 Passelègue, F. X., Goldsby, D. L., & Fabbri, O. (2014). The influence of ambient fault tem-
847 perature on flash-heating phenomena. *Geophysical Research Letters*, 41(3), 828-835.
848 doi: 10.1002/2013GL058374
- 849 Persson, B. N. J. (2000). *Sliding friction, physical principles and applications* (K. von Klitz-
850 ing & R. Wiesendanger, Eds.). New York: Springer-Verlag.

- 851 Poirier, J.-P. (1985). *Creep of crystals: High-temperature deformation processes in metals,*
852 *ceramics and minerals*. Cambridge University Press.
- 853 Pozzi, G., De Paola, N., Holdsworth, R. E., Bowen, L., Nielsen, S. B., & Dempsey, E. D.
854 (2019). Coseismic ultramylonites: An investigation of nanoscale viscous flow and
855 fault weakening during seismic slip. *Earth and Planetary Science Letters*, 516, 164–
856 175.
- 857 Pozzi, G., De Paola, N., Nielsen, S. B., Holdsworth, R. E., & Bowen, L. (2018). A new
858 interpretation for the nature and significance of mirror-like surfaces in experimental
859 carbonate-hosted seismic faults. *Geology*, 46(7), 583–586.
- 860 Proctor, B. P., T. M. Mitchell, T., Hirth, G., Goldsby, D., Zorzi, F., Platt, J., & Di Toro, G.
861 (2014). Dynamic weakening of serpentinite gouges and bare surfaces at seismic slip
862 rates. *J. Geophys. Res. Solid Earth*, 119, 119. doi: 10.1002/2014JB011057
- 863 Raterron, P., Wu, Y., Weidner, D. J., & Chen, J. (2004). Low-temperature olivine rheology at
864 high pressure. *Physics of the Earth and Planetary Interiors*, 145(1), 149-159.
- 865 Rempel, A. W., & Rice, J. R. (2006). Thermal pressurization and onset of melting in fault
866 zones. *J. Geophys. Res.*, 111, B09314. doi: 10.1029/2006JB004314
- 867 Rempel, A. W., & Weaver, S. L. (2008). A model for flash weakening by asperity melting
868 during high-speed earthquake slip. *J. Geophys. Res.*, 113(B11), B11308. doi: 10.1029/
869 2008JB005649
- 870 Rice, J. (1999). Flash heating at asperity contacts and rate-dependent friction. *Eos Trans.*
871 *AGU*, 80(46), F6811. (Fall Meet. Suppl.)
- 872 Rice, J. R. (2006). Heating and weakening of faults during earthquake slip. *J. Geophys. Res.*,
873 111, B05311. doi: 10.1029/2005JB004006
- 874 Ruina, A. (1983). Slip instability and state variable friction laws. *J. Geophys. Res.*, 88,
875 10359-10370.
- 876 Sibson, R. H. (2003). Thickness of the seismic slip zone. *Bulletin of the Seismological Soci-*
877 *ety of America*, 93(3), 1169-1178. doi: 10.1785/0120020061
- 878 Smith, S., Nielsen, S., & Di Toro, G. (2015, Mar). Strain localization and the onset of dy-
879 namic weakening in calcite fault gouge. *Earth Planet. Sci. Lett.*, 413, 25-36. doi: 10
880 .1016/j.epsl.2014.12.043
- 881 Sone, H., & Shimamoto, T. (2009). Frictional resistance of faults during accelerating and de-
882 celerating earthquake slip. *Nature Geoscience*. doi: 10.1038/NGEO637
- 883 Spudich, P. (1998). Use of fault striations and dislocation models to infer tectonic shear

- 884 stress during the 1995 Hyogo-ken Nanbu (Kobe), Japan, earthquake. *Bull. Seismol.*
885 *Soc. Am.*, 88, 413–427.
- 886 Sulem, J., & Famin, V. (2009). Thermal decomposition of carbonates in fault zones: Slip-
887 weakening and temperature limiting effects. *J. Geophys. Res.*, 114, B03309. doi: 10
888 .1029/2008JB006004
- 889 Tisato, N., Di Toro, G., De Rossi, N., Quaresimin, M., & Candela, T. (2012, May). Exper-
890 imental investigation of flash weakening in limestone. *Journal of Structural Geology*,
891 38, 183-199. doi: 10.1016/j.jsg.2011.11.017
- 892 Tsutsumi, A., & Shimamoto, T. (1997). High-velocity frictional properties of gabbro. *Geo-*
893 *phys. Res. Lett.*, 24, pp.699-702.
- 894 Viesca, R. C., & Garagash, D. I. (2015, 10 05). Ubiquitous weakening of faults due to ther-
895 mal pressurization. *Nature Geosci.* (advance online publication) doi: 10.1038/
896 ngeo2554
- 897 Violay, M., Di Toro, G., Nielsen, S., Spagnuolo, E., & Burg, J. (2015). Thermo-mechanical
898 pressurization of experimental faults in cohesive rocks during seismic slip. *Earth*
899 *Planet. Sci. Lett.*, 429, 1 - 10. doi: 10.1016/j.epsl.2015.07.054
- 900 Violay, M., Di Toro, G., Gibert, B., Nielsen, S., Spagnuolo, E., Del Gaudio, P., ... Scarlato,
901 P. G. (2014, Jan). Effect of glass on the frictional behavior of basalts at seismic slip
902 rates. *Geophysical Research Letters*, 41(2), 348-355. doi: 10.1002/2013gl058601
- 903 Violay, M., Gibert, B., Mainprice, D., Evans, B., Dautria, J.-M., Azais, P., & Pezard, P.
904 (2012). An experimental study of the brittle-ductile transition of basalt at oceanic crust
905 pressure and temperature conditions. *Journal of Geophysical Research: Solid Earth*,
906 117(B3). doi: 10.1029/2011JB008884
- 907 Violay, M., Nielsen, S., Cinti, D., Spagnuolo, E., Di Toro, G., & Smith, S. (2011). Friction of
908 marble under seismic deformation conditions in the presence of fluid. In *Agu 2011 fall*
909 *meeting*.
- 910 Violay, M., Nielsen, S., Gibert, B., Spagnuolo, E., Cavallo, A., Azais, P., ... Di Toro, G.
911 (2013). Effect of water on the frictional behavior of cohesive rocks during earth-
912 quakes. *Geology*, 42(1), 27-30. doi: 10.1130/G34916.1
- 913 Violay, M., Nielsen, S., Spagnuolo, E., Cinti, D., Di Toro, G., & Stefano, G. D. (2013).
914 Pore fluid in experimental calcite-bearing faults: Abrupt weakening and geochemi-
915 cal signature of co-seismic processes. *Earth Planet. Sci. Lett.*, 361(0), 74 - 84. doi:
916 10.1016/j.epsl.2012.11.021

- 917 Violay, M., Passelegue, F., Spagnuolo, E., Di Toro, G., & Cornelio, C. (2019). Effect of wa-
 918 ter and rock composition on re-strengthening of cohesive faults during the deceleration
 919 phase of seismic slip pulses. *Earth and Planetary Science Letters*, 522, 55 - 64. doi:
 920 <https://doi.org/10.1016/j.epsl.2019.06.027>
- 921 Weidner, D. J., Wang, Y., & Vaughan, M. T. (1994, May). Yield strength at high pressure and
 922 temperature. *Geophysical Research Letters*, 21(9), 753-756. doi: 10.1029/93gl03549
- 923 Yuan, F., & Prakash, V. (2008). Slip weakening in rocks and analog materials at co-seismic
 924 slip rates. *J. Mech. Phys. Solids*, 56, 542-560.
- 925 Yuan, F., & Prakash, V. (2012, Aug). Laboratory observations of transient frictional slip
 926 in rock-analog materials at co-seismic slip rates and rapid changes in normal stress.
 927 *Tectonophysics*, 558-559, 58-69. doi: 10.1016/j.tecto.2012.06.026
- 928 Zheng, G., & Rice, J. (1998). Conditions under which velocity weakening friction allows a
 929 self-healing versus a cracklike mode of rupture. *Bull. Seismol. Soc. Am.*, 88(6), 1466-
 930 1483.

Figure.

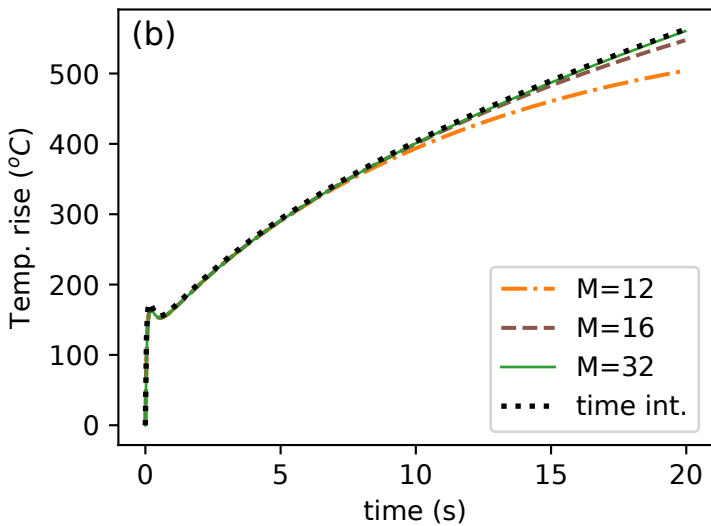
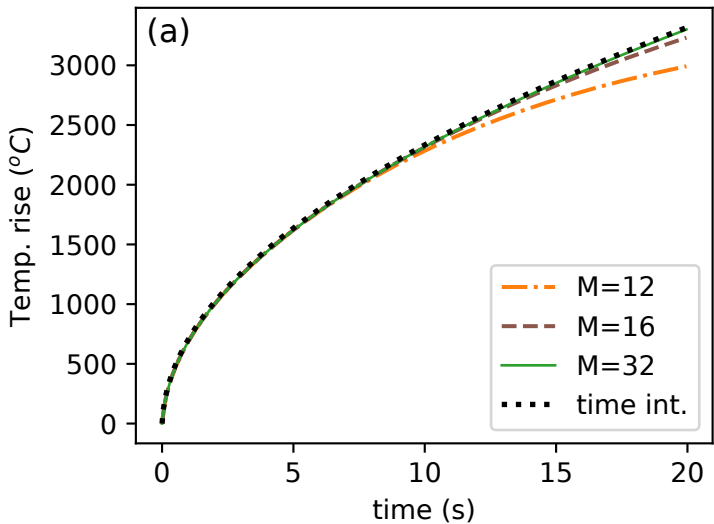
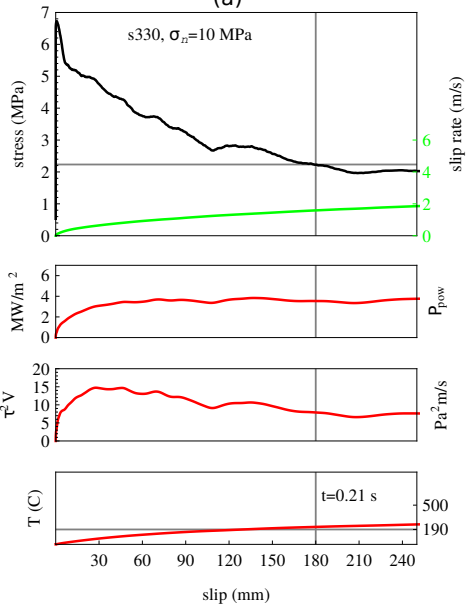


Figure.

(a)



(b)

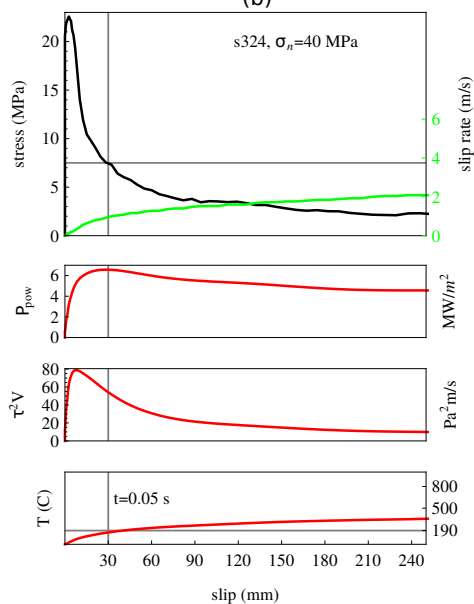


Figure.

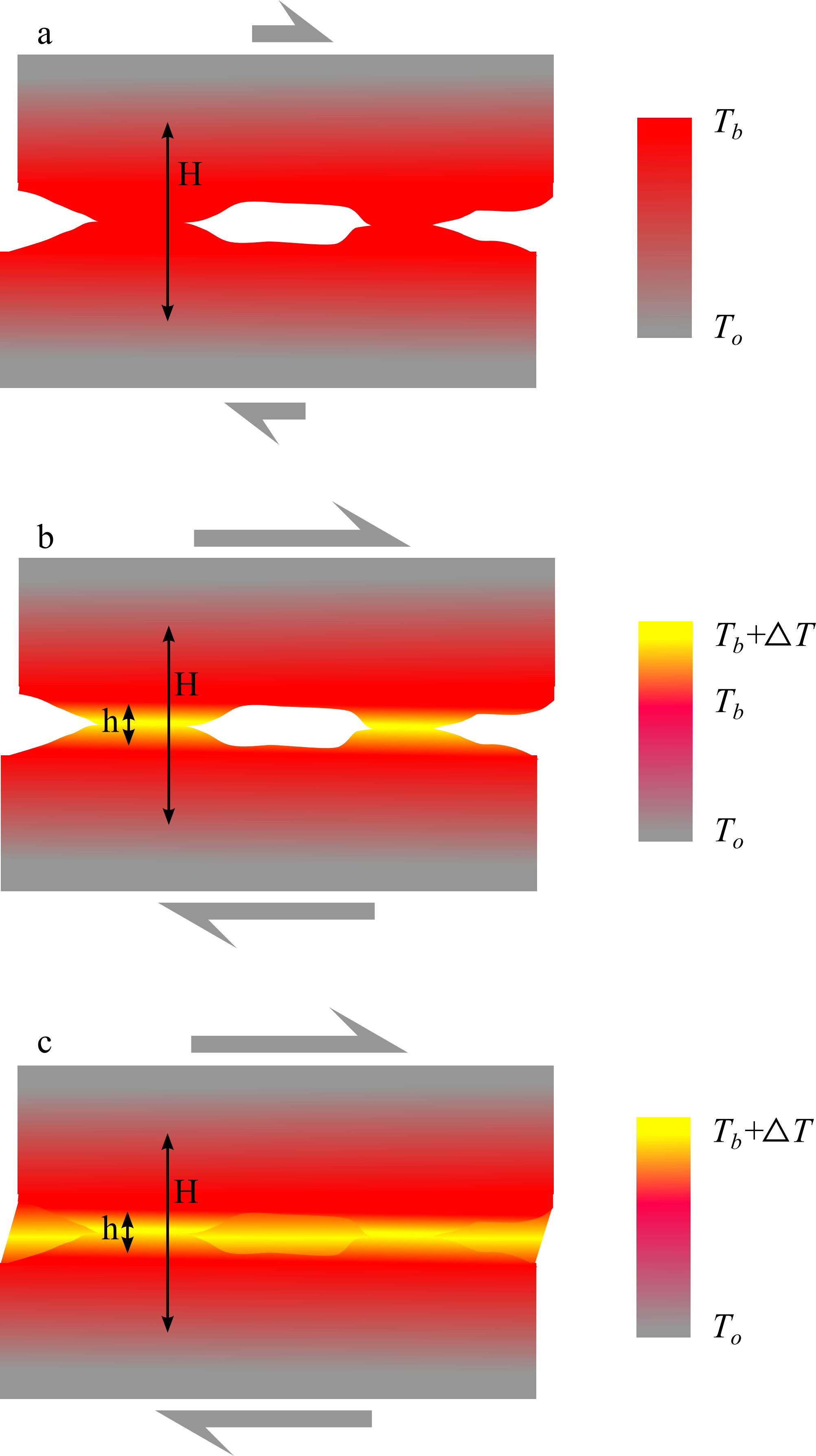


Figure.

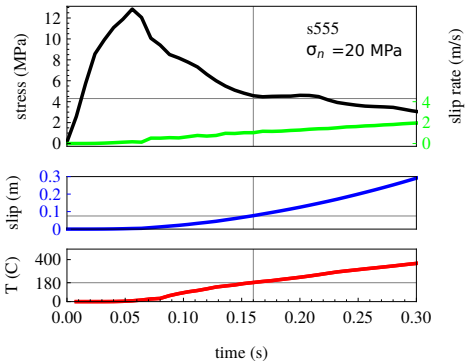


Figure.

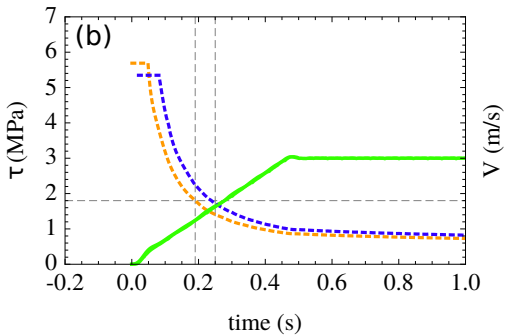
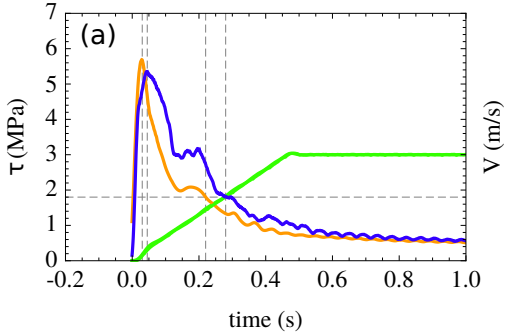


Figure.

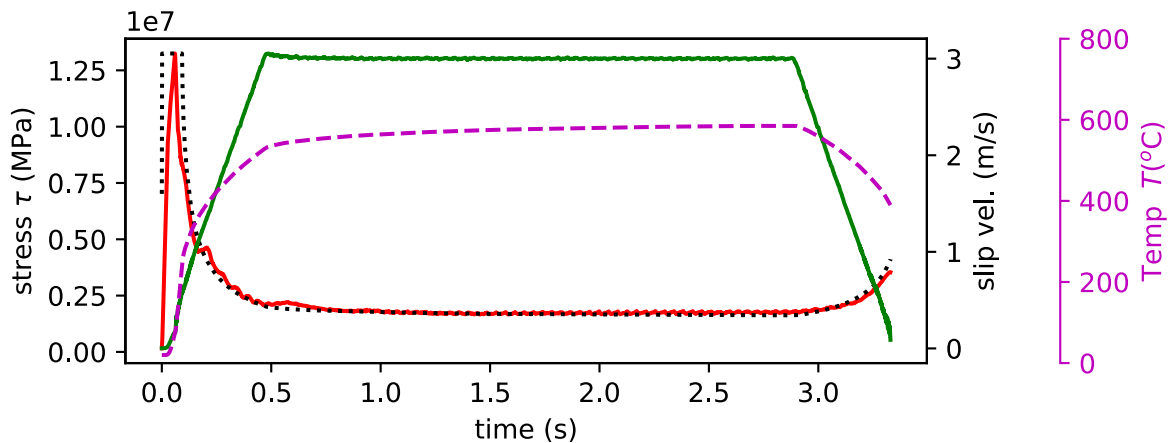
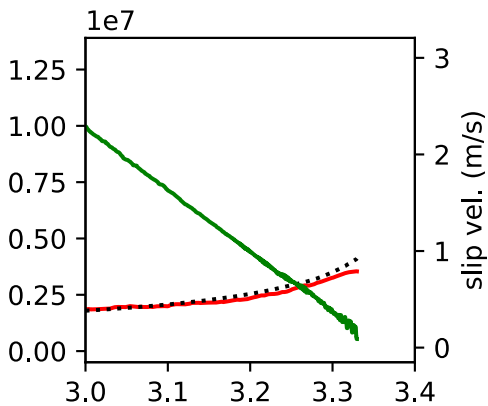
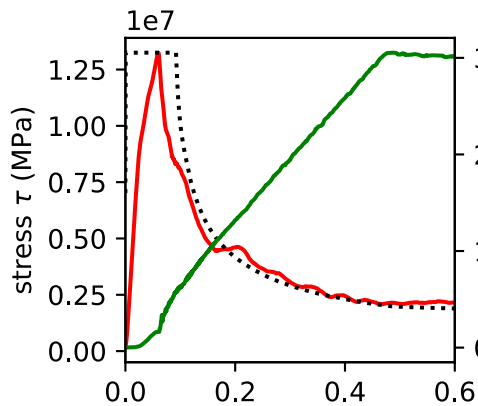


Figure.

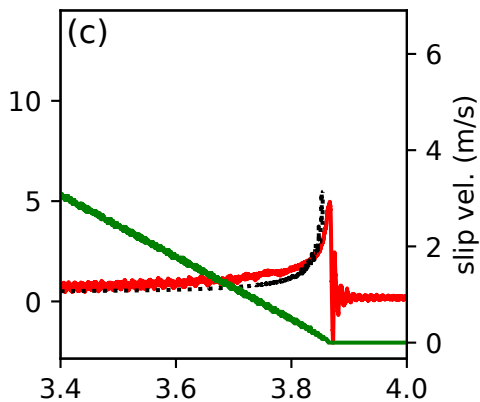
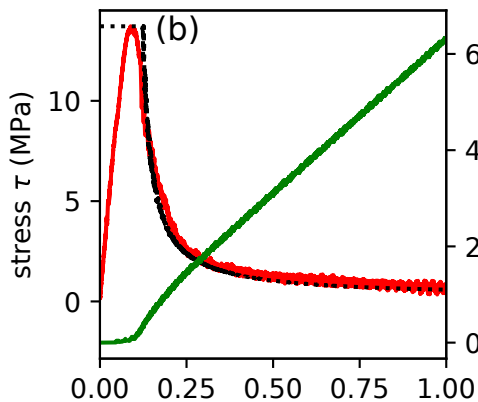
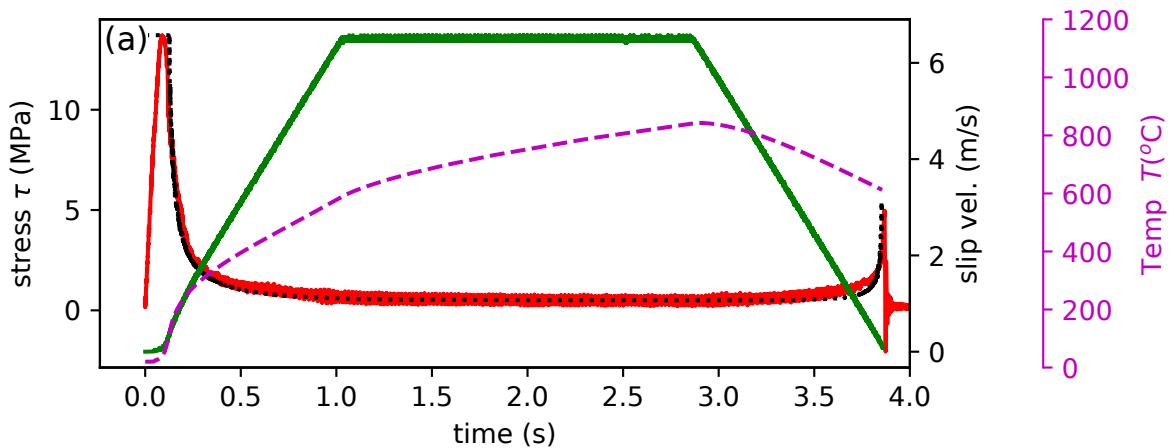


Figure.

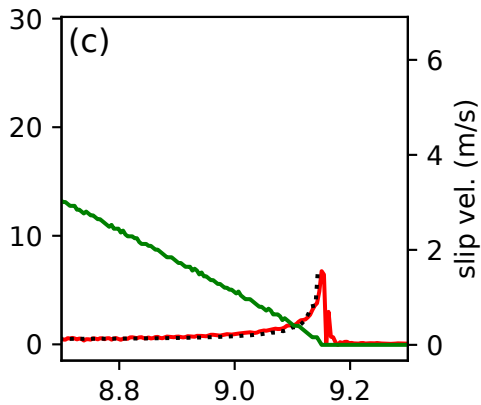
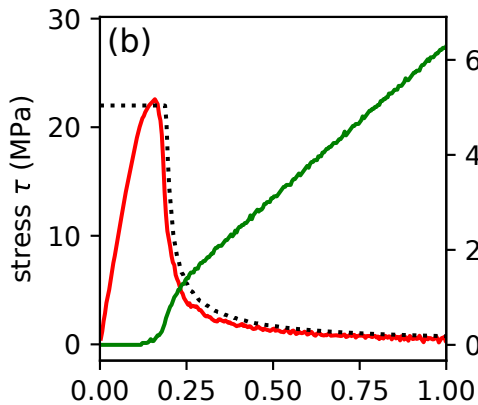
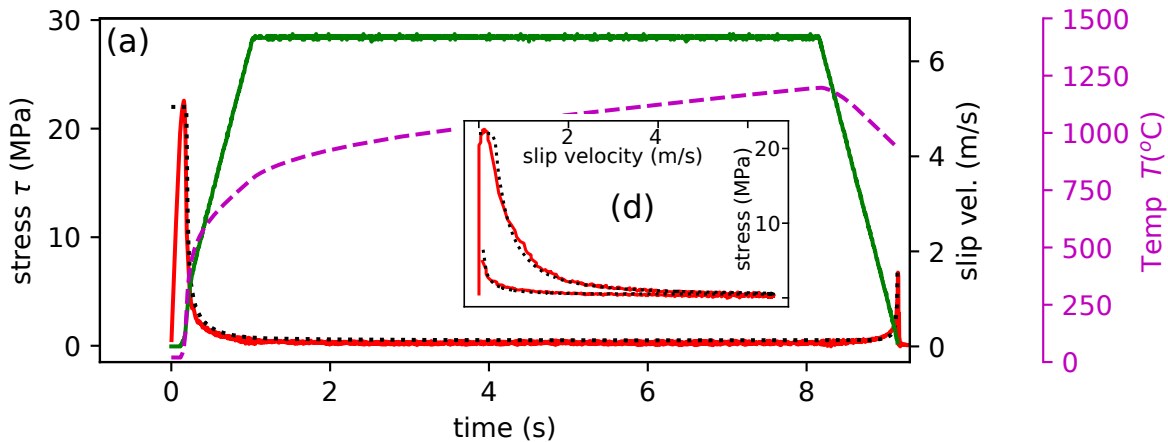


Figure.

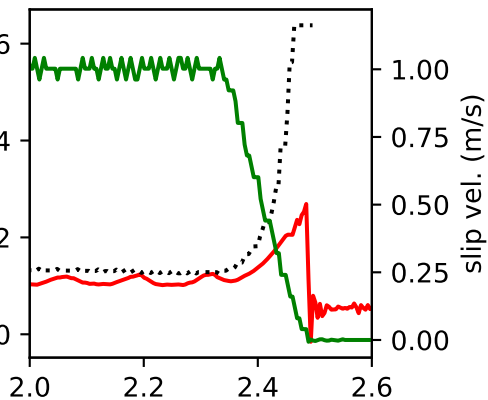
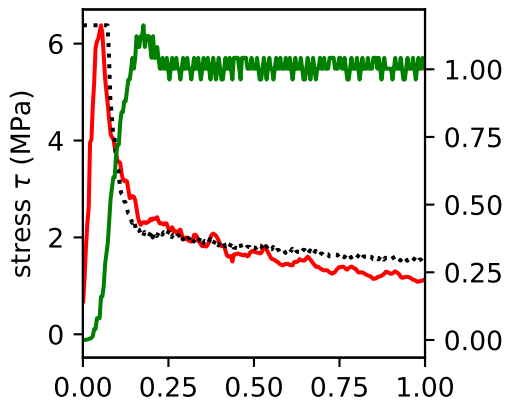
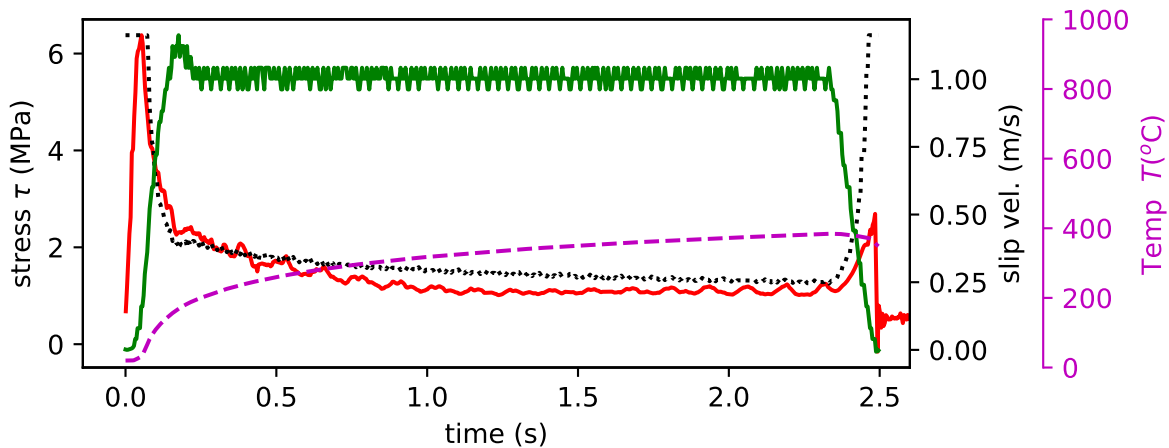


Figure.

